



**NAVAL
POSTGRADUATE
SCHOOL**

MONTEREY, CALIFORNIA

THESIS

**REMOTELY TRIGGERED SOLAR BLIND SIGNALING
USING DEEP ULTRAVIOLET (UV) LEDS**

by

Spencer V. Talley

June 2011

Thesis Advisor:
Second Reader:

Nancy M. Haegel
Richard M. Harkins

Approved for public release; distribution is unlimited

THIS PAGE INTENTIONALLY LEFT BLANK

REPORT DOCUMENTATION PAGE			Form Approved OMB No. 0704-0188
Public reporting burden for this collection of information is estimated to average 1 hour per response, including the time for reviewing instruction, searching existing data sources, gathering and maintaining the data needed, and completing and reviewing the collection of information. Send comments regarding this burden estimate or any other aspect of this collection of information, including suggestions for reducing this burden, to Washington headquarters Services, Directorate for Information Operations and Reports, 1215 Jefferson Davis Highway, Suite 1204, Arlington, VA 22202-4302, and to the Office of Management and Budget, Paperwork Reduction Project (0704-0188) Washington DC 20503.			
1. AGENCY USE ONLY (Leave blank)	2. REPORT DATE June 2011	3. REPORT TYPE AND DATES COVERED Master's Thesis	
4. TITLE AND SUBTITLE Remotely Triggered Solar Blind Signaling Using Deep Ultraviolet (UV) LEDs		5. FUNDING NUMBERS	
6. AUTHOR(S) Spencer V. Talley		8. PERFORMING ORGANIZATION REPORT NUMBER	
7. PERFORMING ORGANIZATION NAME(S) AND ADDRESS(ES) Naval Postgraduate School Monterey, CA 93943-5000		10. SPONSORING/MONITORING AGENCY REPORT NUMBER	
9. SPONSORING /MONITORING AGENCY NAME(S) AND ADDRESS(ES) N/A		11. SUPPLEMENTARY NOTES The views expressed in this thesis are those of the author and do not reflect the official policy or position of the Department of Defense or the U.S. Government. IRB Protocol number N/A.	
12a. DISTRIBUTION / AVAILABILITY STATEMENT Approved for public release; distribution is unlimited		12b. DISTRIBUTION CODE	
13. ABSTRACT (maximum 200 words) The purpose of the triggered individual identification friend or foe (IIFF) patch is to covertly reduce fratricide incidents and provide related remotely triggered marking or signaling capability. This research extended previous work by evaluating solar blind UV light emitting diodes (LEDs). Due to the zero background condition ("solar blind") from 200 to 280 nm, use of a UV source in this 80 nm window can be used to create a triggered IIFF patch that works both day and night. Additionally, due to the strong wavelength dependence for scattering reactions in air, UV light may provide a means to accomplish non line of sight (NLOS) signaling. The goal of this research was to develop a working prototype of a triggered IIFF device that can be seen from a distance of 1 km, either day or night, and explore the possibility of using this device to perform NLOS signaling. Results will be presented demonstrating prototype performance in a field exercise, as well as the device characterization required to define and optimize the prototype design. Device characterization included measurements of LED intensity as a function of driving current and voltage and the determination of LED performance parameters outside the standard operating specifications.			
14. SUBJECT TERMS Solar blind ultraviolet, fratricide, intensity		15. NUMBER OF PAGES 89	
		16. PRICE CODE	
17. SECURITY CLASSIFICATION OF REPORT Unclassified	18. SECURITY CLASSIFICATION OF THIS PAGE Unclassified	19. SECURITY CLASSIFICATION OF ABSTRACT Unclassified	20. LIMITATION OF ABSTRACT UU

THIS PAGE INTENTIONALLY LEFT BLANK

Approved for public release; distribution is unlimited

**REMOTELY TRIGGERED SOLAR BLIND SIGNALING USING DEEP
ULTRAVIOLET (UV) LEDS**

Spencer V. Talley
Lieutenant, United States Navy
B.S., Weber State University, 2004

Submitted in partial fulfillment of the
requirements for the degree of

MASTER OF SCIENCE IN PHYSICS

from the

**NAVAL POSTGRADUATE SCHOOL
June 2011**

Author: Spencer V. Talley

Approved by: Nancy M. Haegel
Thesis Advisor

Richard M. Harkins
Second Reader

Andres Larraza
Chairman, Department of Physics

THIS PAGE INTENTIONALLY LEFT BLANK

ABSTRACT

The purpose of the triggered individual identification friend or foe (IIFF) patch is to covertly reduce fratricide incidents and provide related remotely triggered marking or signaling capability. This research extended previous work by evaluating solar blind UV light emitting diodes (LEDs). Due to the zero background condition (“solar blind”) from 200 to 280 nm, use of a UV source in this 80 nm window can be used to create a triggered IIFF patch that works both day and night. Additionally, due to the strong wavelength dependence for scattering reactions in air, UV light may provide a means to accomplish non line of sight (NLOS) signaling.

The goal of this research was to develop a working prototype of a triggered IIFF device that can be seen from a distance of 1 km, either day or night, and explore the possibility of using this device to perform NLOS signaling. Results will be presented demonstrating prototype performance in a field exercise, as well as the device characterization required to define and optimize the prototype design. Device characterization included measurements of LED intensity as a function of driving current and voltage and the determination of LED performance parameters outside the standard operating specifications.

THIS PAGE INTENTIONALLY LEFT BLANK

TABLE OF CONTENTS

I.	INTRODUCTION.....	1
A.	BACKGROUND	1
B.	NEAR IR AND SHORT WAVE IR IIFF PATCHES	3
C.	PROJECT SCOPE.....	5
II.	SOLAR BLIND AND ZERO SOLAR BACKGROUND RADIATION.....	7
A.	SOLAR BLIND ULTRAVIOLET RADIATION	7
B.	ZERO SOLAR BACKGROUND RADIATION.....	10
III.	DETERMINATION AND EVALUATION OF SOLAR BLIND UV SOURCE.....	15
A.	POSSIBLE SOLAR BLIND UV SOURCES.....	15
B.	INTENSITY LOSSES	17
C.	INITIAL INTENSITY MEASUREMENTS	18
D.	INTENSITY DISTRIBUTION MEASUREMENTS.....	20
E.	EVALUATION OF 270 NM HS LED.....	22
F.	SUMMARY	27
IV.	LED PERFORMANCE OUTSIDE RECOMMENDED OPERATING PARAMETERS.....	29
A.	RECOMMENDED OPERATING PARAMETERS	29
B.	CURRENT MEASUREMENTS AS A FUNCTION OF BIAS VOLTAGE.....	29
C.	INTENSITY MEASUREMENTS AS A FUNCTION OF CURRENT.....	31
D.	TRANSIENT INTENSITY MEASUREMENTS.....	35
E.	EVALUATION OF PERFORMANCE FOR OPERATION OUTSIDE OF RECOMMENDED OPERATING PARAMETERS.....	40
F.	SUMMARY	43
V.	SCATTERING AND NONLINE OF SIGHT DETECTION.....	45
A.	RAYLEIGH SCATTERING	45
B.	NLOS DETECTION USING LOCK-IN TECHNIQUES.....	47
C.	NLOS IMAGING.....	50
D.	SUMMARY AND CONCLUSION	51
VI.	SOLAR BLIND UV IIFF PROTOTYPE PERFORMANCE AND CONCLUSION	53
A.	PROTOTYPE DESIGN	53
B.	PROTOTYPE PERFORMANCE AND EVALUATION	54
C.	CONCLUSIONS AND SUGGESTIONS FOR FUTURE WORK.....	56
	APPENDIX. SUPPLEMENTAL	59
	LIST OF REFERENCES.....	69
	INITIAL DISTRIBUTION LIST	71

THIS PAGE INTENTIONALLY LEFT BLANK

LIST OF FIGURES

Figure 1.	Wearable infrared beacon (Powerflare, Inc.).....	2
Figure 2.	Infrared retro-reflective patches with U.S. markings (Night Vision Systems).....	2
Figure 3.	Individual Identification Friend or Foe (IIFF) patch.	3
Figure 4.	NVD test and SWIR comparison of triggered SWIR IIFF patch response (From [6]).....	5
Figure 5.	Ozone absorption cross-section from 200 – 300 nm (From [7]).	8
Figure 6.	Normalized intensity spectrum of the sun based on Planck’s law for blackbody radiation at 5770 K.....	9
Figure 7.	Measured spectrum from Sun, 275 nm LED, and 255 nm LED.....	10
Figure 8.	%Transmission curves for solar blind bandpass filters used to achieve zero solar background radiation condition. Left: 270 nm broadband filter (270B). Right: 270 nm narrowband filter (270N) (From [9]).....	11
Figure 9.	Close-up view of mount used to hold LED.	12
Figure 10.	270 nm LED in “off” (left) and “on” (right) conditions as viewed by visible camera with zero responsivity in the ultraviolet.	12
Figure 11.	270 nm LED in “off” (left) and “on” (right) conditions as viewed by intensified PentaMAX camera sensitive to both ultraviolet and visible light.	13
Figure 12.	270 nm LED in “on” condition as seen from 5m by a camera sensitive to both ultraviolet and visible light using a 270 nm bandpass filter.	13
Figure 13.	UVTOP [®] LEDs from Sensor Electronic Technology Inc. From Left to right: Flat Widow, Ball Lens, and Hemispherical Lens models of 270 nm LEDs.	15
Figure 14.	A schematic diagram of a typical AlGaIn – based light emitting diode (From [12]).....	16
Figure 15.	Responsivity of FGAP71 GaP Photodiode as a function of wavelength (From [14]).....	18
Figure 16.	Setup used to measure intensity of various deep UV LED types.	19
Figure 17.	Measured intensities of LED models.....	19
Figure 18.	Emission patterns for UVTOP [®] LED lenses (From [15]).	20
Figure 19.	Setup used to measure angular dependence of intensity.....	21
Figure 20.	Normalized intensity as a function of LED angle. Initial point for hemispherical lens and ball lens LEDs overlap.	22
Figure 21.	Circuit diagram of first mobile test device.	23
Figure 22.	Daytime image of single 270 nm HS LED with 20 mA driving current viewed from 100 m through 270N and 270B solar blind filters with 50 ms integration time.	24
Figure 23.	Nighttime images of single 270 nm HS LED with 20 mA driving current. Left: Viewed from 100 m through 270B solar blind filter with 20 ms exposure time. Right: Viewed from 300 m through 270B solar blind filter with 100 ms exposure time.	25

Figure 24.	MATLAB plots of images from Figure 9. Top: 270 nm HS LED with 20 mA driving current viewed from 100 m with 20 ms exposure time. Bottom: 270 nm HS LED with 20 mA driving current viewed from 300 m with 100 ms exposure time.	26
Figure 25.	Current as a function of bias voltage for 270 nm LEDs of each lens type.	30
Figure 26.	Setup used to measure intensity as a function of current.	31
Figure 27.	Intensity as a function of current for 270 nm HS LED.	32
Figure 28.	Intensity as a function of current for 270 nm BL LED.	33
Figure 29.	Intensity as a function of current for 270 nm FW LED.	34
Figure 30.	Normalized power as a function of temperature for UVTOP [®] 270 nm LEDs. Normalized power = 1.0 at 25°C (From [15]).	35
Figure 31.	Setup used to measure LED intensity as a function of time.	36
Figure 32.	Intensity as a function of time for 270 nm HS LED at constant current.	37
Figure 33.	Electroluminescence spectra of 277 nm LEDs under different currents. For current ≥ 50 mA a 10 μ s pulse was used (From [12]).	38
Figure 34.	Intensity as a function of time for 270 nm HS LED pulsed current.	39
Figure 35.	Comparing intensity as a function of time of 270 nm HS LED for 120 mA DC current vs. 120 mA pulsed current.	40
Figure 36.	Circuit diagram of second mobile test device.	41
Figure 37.	Daytime image of four 270 nm HS LEDs each with 70 mA driving current viewed from 300 m through 270N and 270B solar blind filters with 150 ms exposure time.	42
Figure 38.	Nighttime image of four 270 nm HS LEDs each with 70 mA driving current viewed from 300 m through 270B solar blind filter with 150 ms exposure time.	43
Figure 39.	Example of NLOS imaging. UV light being scattered through chalk dust. ..	45
Figure 40.	Due to the higher rate of scattering for UV light, it may be possible to perform NLOS detection or signaling. Scattering reactions in the air send photons in all directions. Some of these will propagate toward the observer, providing a means of visual communication even if the direct path is blocked.	46
Figure 41.	Setup used to measure intensity of UV light due to Rayleigh scattering.	47
Figure 42.	Scattered intensity as a function of detector angle for first measurement set ($d_1 = d_2 = 6$ in).	49
Figure 43.	Scattered intensity as a function of detector angle for second measurement set ($d_1 = 12$ in; $d_2 = 6$ in). The irregularities for angles less than 20° are because a significant fraction of the detector's field of view does not contribute to intensity for small angles for this relative position between the source and receiver.	49
Figure 44.	Scattered intensity as a function of detector angle for third measurement set ($d_1 = 6$ in; $d_2 = 12$ in).	50
Figure 45.	Attempt to view scattering of UV photons in air.	51
Figure 46.	Solar blind UV IIFF prototype device.	53
Figure 47.	Daytime images of prototype device viewed from 980 m by visible camera (Top) and intensified PentaMAX camera with 270N and 270B	

Figure 48. solar blind filters and 30 ms exposure time (bottom). In the second image, the prototype is the white dot shown just below the horizon.....55
Nighttime image of prototype device viewed from 980 m with 20 ms exposure time.....56

THIS PAGE INTENTIONALLY LEFT BLANK

LIST OF ACRONYMS AND ABBREVIATIONS

270B	270 nm broadband filter
270N	270 nm narrowband filter
BL	Ball lens
FW	Flat window
HS	Hemispherical lens
IIFF	Individual identification friend or foe
IR	Infrared
LED	Light emitting diode
LOS	Line of sight
LWIR	Long wave infrared
NG-NVD	Next generation night vision device
NIR	Near infrared
NLOS	Nonline of sight
NVD	Night vision device
OSD	Office of the Secretary of Defense
PMT	Photomultiplier tube
P-OLED	Polymer light emitting diode
SETI	Sensor electronic technology corporation
SWIR	Short wave infrared
TRADOC	U.S. Army Training and Doctrine Command
USSOCOM	U.S. Special Operations Command
UV	Ultraviolet

THIS PAGE INTENTIONALLY LEFT BLANK

ACKNOWLEDGMENTS

This work was made possible through the funding provided by the USSOCOM-NPS Field Experimentation program and the Office of Naval Research Code 30.

I would like to thank Sam Barone for his assistance fixing the UV sensitive camera, which was vital to my research. Also, thank you to George Jaksha for machining important parts that were used over and over again.

Thank you to Bill Cross at Syvax Design. Not only did he also fix the UV sensitive camera, but he also designed the driving and detection circuitry for the prototype.

Thank you to Dr. Richard Harkins for teaching me how to operate the UV camera and the software that goes with it. Also, thank you for helping guide my academic curriculum for the past two years.

Dr. Nancy Haegel helped me in every step of this project, and for that, I will be forever grateful to her. Thank you for your suggestions on how to get the data I wanted and also how to present it.

Of course, I owe my gratitude to my family. To my wife, Mayra, and my children, Ally, Anna, and Ethan, for being willing to share me with this research. This would not have been possible without your support.

THIS PAGE INTENTIONALLY LEFT BLANK

I. INTRODUCTION

A. BACKGROUND

According to U.S. Army TRADOC Fratricide Action Plan, "Fratricide is the employment of friendly weapons and munitions with the intent to kill the enemy or destroy his equipment, or facilities, which results in unforeseen and unintentional death or injury to friendly personnel" [1]. Although fratricide has always been a problem in armed combat, advancements in technology have resulted in increasingly lethal weapons that can be used from greater distances, even in ground-to-ground combat. In addition, the speed and complexity of combat has increased. This can make it difficult to distinguish between friendly and nonfriendly forces.

In the 1991 Operation Desert Storm, friendly fire incidents accounted for 24% of U.S. casualties. Of these fratricide incidents, 61% involved ground-to-ground incidents [2]. This number increased to new levels in the 2003 Operation Iraqi Freedom, where 'blue-on-blue' engagement accounted for 45% of U.S. casualties. Again, 61% of these incidents resulted from ground-to-ground engagements [3].

As the battlefield becomes more complex, new technology is needed to covertly identify friendly forces. The two prominent means of fratricide prevention for ground-to-ground engagement currently in use are infrared (IR) beacons and infrared reflective patches. The IR beacons (Figure 1) work by emitting a blinking IR signal whenever they are turned on. Because they operate in the IR, they are only effective during nighttime operations. In addition, although they can serve to identify friendly personnel, the IR beacons are not covert. The emitted IR light can be seen by anyone using a night vision device (NVD), friendly or not. Therefore, use of these beacons may inadvertently reveal the wearer's position to enemy forces



Figure 1. Wearable infrared beacon (Powerflare, Inc.).

The IR reflective patches (Figure 2) are small, wearable patches made from “glint tape.” They are designed to reflect any incident IR light back to the source. A major advantage of these patches is that unlike the IR beacons, they are not constantly “advertising” the wearer’s position. They must be illuminated by an IR source such as a targeting laser or beacon source in order to be visible. However, these patches are indiscriminant in that the reflection does not distinguish between friendly or unfriendly illumination.



Figure 2. Infrared retro-reflective patches with U.S. markings (Night Vision Systems).

B. NEAR IR AND SHORT WAVE IR IIFF PATCHES

In 2009, the Office of the Secretary of Defense (OSD) directed the Technology Transition Initiative (TTI) program to fund the Polymer Light Emitting Diode (P-OLED) Enabled Individual Identification Friend or Foe (IIFF) project [4]. In response to this direction, and in order to provide a covert solution for fratricide mitigation, a series of triggered IR IIFF patches have been developed at Naval Postgraduate School.



Figure 3. Individual Identification Friend or Foe (IIFF) patch.

These patches make use of a triggering mechanism that allows them to behave passively and therefore covertly. Special sensors built into the patch are able to detect laser targeting and illumination from friendly ground troops. Once it senses that a friendly shooter has targeted it, the patch responds automatically by emitting a flashing IR signal. This signal warns the shooter that they have mistakenly targeted a friendly soldier in time to allow them to disengage. Unlike reflective patches, these IR IIFF patches do not respond to unfriendly engagers or generic IR radiation from sources in the environment.

The more recent models of the IR IIFF patches are able to operate in one of two modes: passive or beacon. While in passive mode, the patch remains covert unless

triggered by a friendly target. Should the need for enhanced situational awareness arise, the patch may be placed in beacon mode. While in beacon mode the patch continuously flashes, emitting an IR signal until turned off.

The first generations of the triggered IR IIFF patches used light from the near infrared (NIR) region of the spectrum, 0.7-1.0 μm . Although the implementation of a triggering mechanism made these models more covert than either the IR reflective patches or IR beacons, as with these current means of fratricide prevention these versions of the triggered IR IIFF patch were visible to generation III NVDs.

The most recent demonstration of the IIFF patch uses emission in the short wave infrared (SWIR) region, 1.0-3.0 μm . This makes the device even more covert because SWIR photons are invisible to the GaAs based generation III NVDs. The patch uses a method known as downconversion to change the wavelength of the emitted photons from the NIR to the SWIR region of the spectrum [5]. Filters are used to eliminate any visible or NIR light, allowing only the SWIR photons to be emitted [6]. Only next-generation NVDs (NG-NVDs) are capable of seeing the emitted SWIR photons. Unlike generation III NVDs, NG-NVDs are still in the relatively early stage of development and are not widely proliferated, making a SWIR device more covert. Figure 4 shows an illuminated SWIR IIFF patch as viewed by both generation III NVDs and a SWIR camera; the patch is invisible to the NVDs, but clearly seen by the SWIR camera.

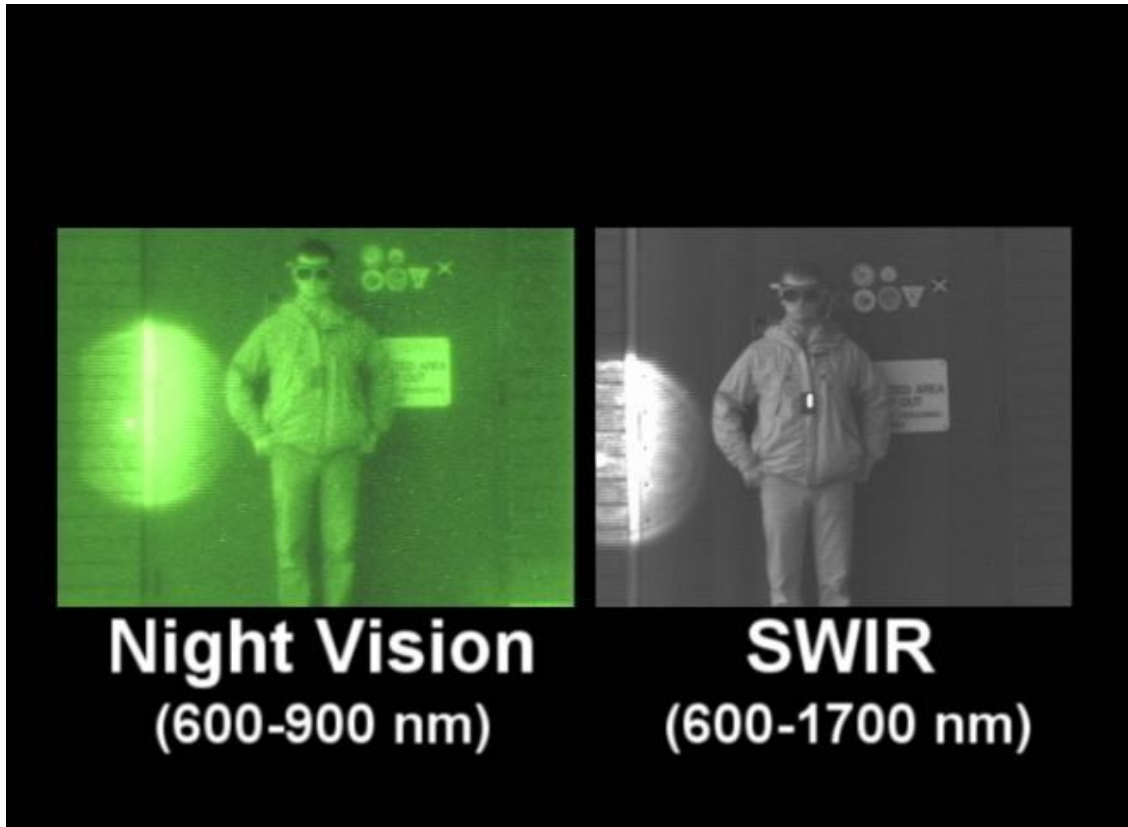


Figure 4. NVD test and SWIR comparison of triggered SWIR IIFF patch response (From [6]).

C. PROJECT SCOPE

The next step is to explore the viability of a triggered solar blind UV patch. Use of solar blind UV light, 200-280 nm, offers the possibility of a device that could produce covert identification or marking and signaling during both day and night. As is the case with SWIR, the capability for UV imaging is not widely available. In addition, due to the increase in molecular scattering of photons of shorter wavelengths, the possibility also exists for performing nonlinear of sight (NLOS) communication and signaling. The goal of this research is to demonstrate proof of concept for a triggered solar blind UV patch that is visible at a range of 1 km during both day and night and to explore the prospect of NLOS signaling.

THIS PAGE INTENTIONALLY LEFT BLANK

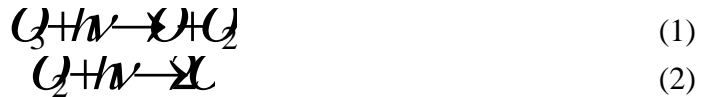
II. SOLAR BLIND AND ZERO SOLAR BACKGROUND RADIATION

A. SOLAR BLIND ULTRAVIOLET RADIATION

Current military applications utilizing the UV portion of the electromagnetic spectrum (~9nm-400nm) include missile detection for aircraft and remote sensing for chemical and biological agents. As the technology advances, many new applications will doubtlessly present themselves. Sources of UV radiation, as well as UV detection, will become cheaper, more efficient and more widely deployed.

Of major interest in military applications is the UVC portion of the spectrum, also known as the solar blind region (200-280 nm). This is called the solar blind region because on and near the earth's surface there is what is referred to as zero solar background radiation for this part of the spectrum. This provides a unique communications opportunity because limitations due to background radiation have been removed.

The solar blind condition occurs because the ozone layer of the upper atmosphere (nominally 20 km altitude) strongly absorbs solar radiation from the following reactions:



This produces zero background conditions in the lower atmosphere and at the earth's surface.

Ozone, O₃, is particularly good at absorbing photons between 230 and 280 nm (Equation 1). Below 230 nm, it is the molecular oxygen, O₂, which primarily determines the amount of absorption (Equation 2). Figure 5 shows the ozone absorption cross section as a function of wavelength in the region from 200-300 nm.

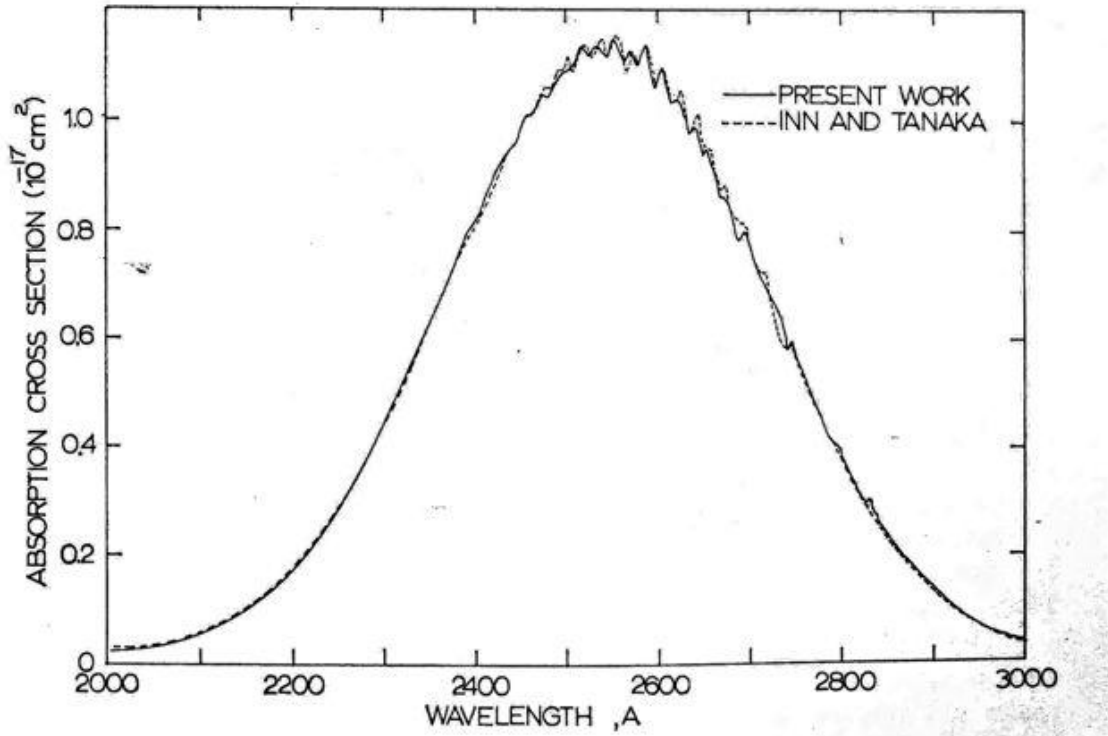


Figure 5. Ozone absorption cross-section from 200 – 300 nm (From [7]).

The free oxygen atoms from each of the above reactions combine with O_2 to form more ozone and the cycle repeats. These reactions absorb 98% of the incident UV radiation. Of the UV light that does pass through the ozone layer, 99% is UVA (320-400 nm). The other 1% is UVB (280-320 nm). Virtually none of the UVC, or solar blind, reaches the lower portions of the earth's atmosphere.

As do all objects with a temperature above absolute zero, the sun emits a broad spectrum of wavelengths. Although not a perfect blackbody, the sun can be modeled as one. Planck's Law, given by Equation 3, produces the plot in Figure 6 as the emission spectrum of the sun at a surface temperature of 5770 K.

$$I(\lambda, T) = \frac{2hc^2}{\lambda^5} \left(\frac{1}{e^{hc/\lambda kT} - 1} \right) \quad (3)$$

where I is the intensity as a function of the wavelength, λ , and the temperature, T , h is Planck's constant, k is Boltzmann's constant, and c is the speed of light.

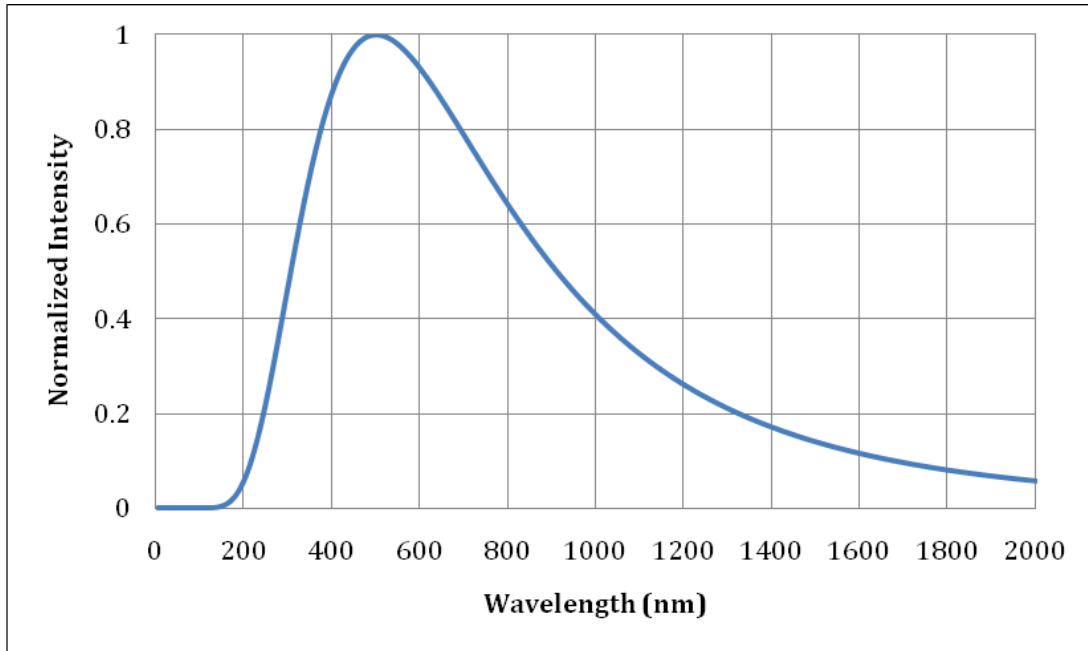


Figure 6. Normalized intensity spectrum of the sun based on Planck's law for blackbody radiation at 5770 K.

Wien's displacement law gives the peak wavelength of blackbody emission and is given by Equation 4.

$$\lambda_{\text{max}} T = 29 \times 10^6 \text{ nmK} \quad (4)$$

For an object of temperature $T = 5770 \text{ K}$, the peak emission per unit wavelength occurs at 503 nm , which is located in the green part of the visible region of the spectrum. Using Equation 3 to calculate the ratio of the solar intensity at 270 nm to the peak intensity gives $\frac{I_{270}}{I_{\text{max}}} = 0.309$. Clearly, the amount of solar blind radiation emitted from the sun is not negligible. However, Figure 7 shows an actual emission spectrum from the sun taken on the earth's surface by an Ocean Optics USB4000-UV-VIS spectrometer. The figure also includes laboratory spectrum of two solar blind LEDs with wavelengths of 255 nm and 270 nm taken with the same spectrometer.

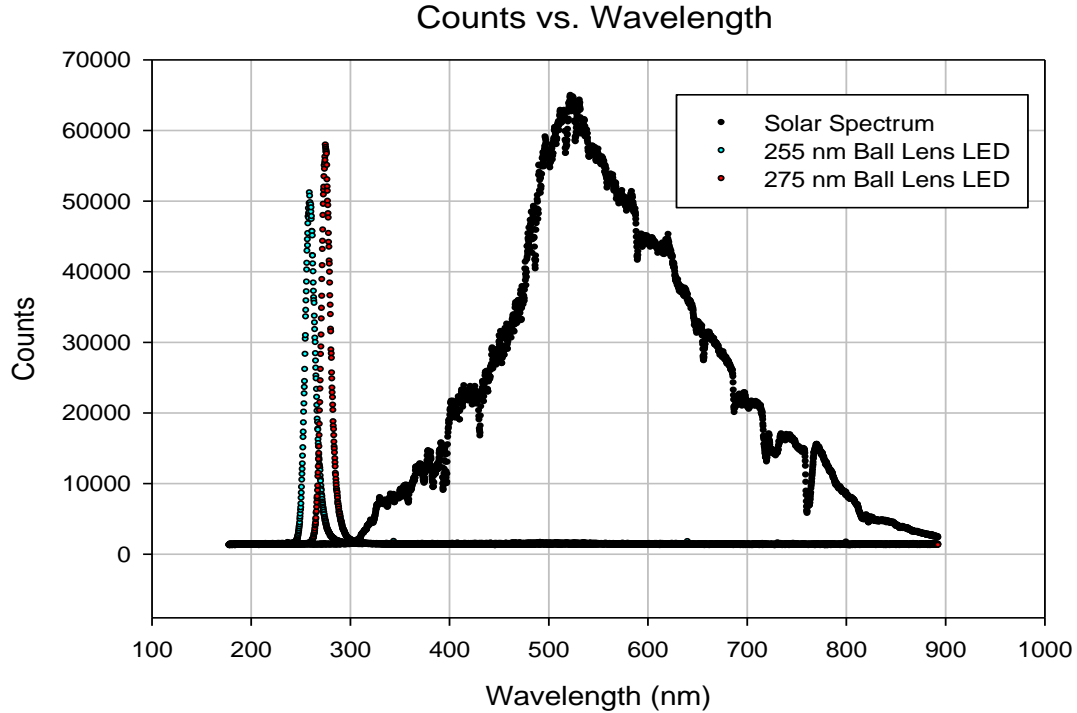


Figure 7. Measured spectrum from Sun, 275 nm LED, and 255 nm LED.

It can be clearly seen that for wavelengths below 300 nm and above 900 nm the measured intensity decreases significantly faster than the blackbody distribution. With respect to the higher wavelengths this is due to the poor sensitivity of the detector. The spectrometer has a range of 200-850 nm and a sensitivity of 130 photons/count at 400 nm and 60 photons/count at 600 nm [8]. Although there is of course significant solar IR radiation at the earth’s surface, the detector used does not respond to it. However, this is not the cause of the absence of solar blind radiation. As is evidenced by the peaks produced by the LEDs, the detector does maintain responsivity in this range, and the lack of measured signal demonstrates the ozone absorption as discussed.

B. ZERO SOLAR BACKGROUND RADIATION

To take advantage of the opportunity for “zero” background presented by using the solar blind UV region of the spectrum, light from other regions of the spectrum must be filtered. One way to accomplish this is using a detector that is only sensitive to the

desired wavelengths. For example, if the detector had a band gap > 4 eV, only photons with wavelengths under 310 nm would have sufficient energy to cause an electron to jump from the valence band to the conduction band and therefore be detected. Use of a wide band gap detector could effectively eliminate all background radiation outside the solar blind region.

The intensified PentaMAX camera used in this research is sensitive to photons from 180-800 nm. Because of this, the zero background radiation condition was achieved through the use of solar blind optical bandpass filters. Two bandpass filters obtained from Acton Optics were used in this research; one narrowband filter (270N) and one broadband filter (270B) each with peak transmission wavelengths close to 270 nm. The narrowband filter offers a minimum peak transmission of 23.5% and a visible rejection of 10^{-4} . The broadband filters provide a minimum peak transmission of 42.3% and a visible rejection of 10^{-2} to 10^{-4} [9]. Figure 8 shows the %transmission curves for each of the filters.

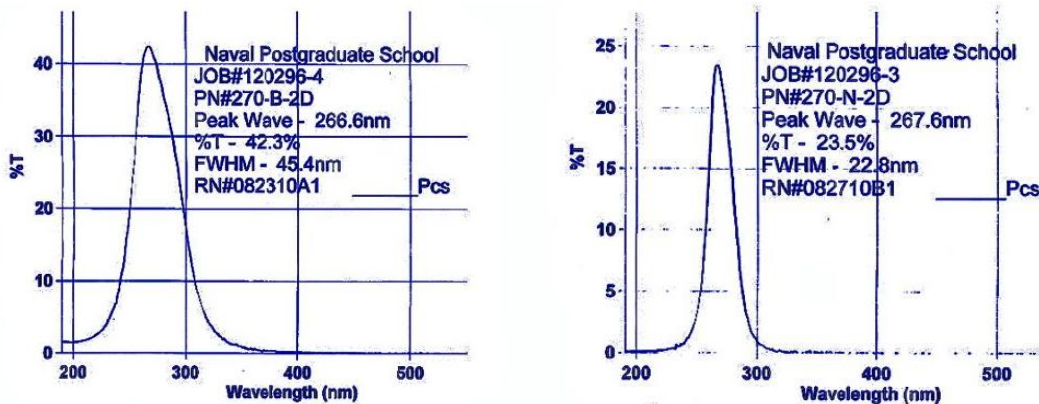


Figure 8. % Transmission curves for solar blind bandpass filters used to achieve zero solar background radiation condition. Left: 270 nm broadband filter (270B). Right: 270 nm narrowband filter (270N) (From [9]).

To illustrate the zero background advantage with a solar blind UV device, a UV LED with a peak emission wavelength of 270 nm was placed in the mount shown in Figure 9 and viewed from a distance of approximately 5 meters.



Figure 9. Close-up view of mount used to hold LED.

Figure 10 compares the LED in both the “off” and “on” conditions viewed through a visible camera with no UV imaging capability.



Figure 10. 270 nm LED in “off” (left) and “on” (right) conditions as viewed by visible camera with zero responsivity in the ultraviolet.

Note that the visible camera does not distinguish between the “on” and “off” condition of the UV LED. This is evidence that a UV emitter would be covert, and minimize the risk of compromising the user’s position due to observation in the visible part of the spectrum. Figure 11 compares the LED in the “off” and “on” condition, but as viewed through an intensified PentaMAX camera.



Figure 11. 270 nm LED in “off” (left) and “on” (right) conditions as viewed by intensified PentaMAX camera sensitive to both ultraviolet and visible light.

Although the intensified PentaMAX camera is able to detect the emitted UV light, the signal is not prominent due to the background radiation in the visible part of the spectrum. Figure 12 shows a final image of the LED in the “on” condition as seen by the intensified PentaMAX camera through a 270 nm bandpass filter.



Figure 12. 270 nm LED in “on” condition as seen from 5m by a camera sensitive to both ultraviolet and visible light using a 270 nm bandpass filter.

With the visible light reduced by a factor of roughly 10^{-4} , the advantage of zero background can be clearly seen. In each image, the driving current of the LED is the same. Although the source is no brighter than before, the absence of background light adds dramatic contrast, which makes the light appear many times brighter.

In the solar blind region of the spectrum, there is zero background radiation both day and night. Because of this, an IIFF device operating in the solar blind region of the spectrum could reduce ground-to-ground fratricide casualties during both day and night operations.

III. DETERMINATION AND EVALUATION OF SOLAR BLIND UV SOURCE

A. POSSIBLE SOLAR BLIND UV SOURCES

To exploit the solar blind region for the purpose of developing an IIFF patch or signaling device, there are many design constraints to consider. These include size, cost, and mobility. The UV source as well as the power supply must be small enough to be worn by a soldier without impacting the soldier's capacity to perform their duties.

Over the past four decades new UV sources such as xenon flashtubes, UV lasers, and mercury-xenon lamps have been developed. All are capable of producing light in the solar blind region [10]. However, these UV systems are expensive, bulky, or inefficient. None of them could serve as the light source for the intended UV IIFF patch. Nevertheless, recent advances in semiconductor UV sources have produced UV LEDs that offer relatively low cost and power consumption, as well as small size [11].

The Sensor Electronic Technology Corporation (SETI) produces a line of commercially available UV LEDs with peak emission wavelengths every 5 nm from 240 -400 nm. In addition, there is the option for one of three different lenses: flat window (FW), ball (BL), and hemispherical (HS). The major difference between the three devices is the emission pattern and divergence of the beam as it leaves the lens. Examples of LEDs of each lens type are shown in Figure 13.



Figure 13. UVTOP[®] LEDs from Sensor Electronic Technology Inc. From Left to right: Flat Window, Ball Lens, and Hemispherical Lens models of 270 nm LEDs.

The UVTOP[®] series of LEDs offered by SETI are a series of AlGaN/AlInGaN based UV and deep-UV LEDs. The wide and direct energy band of III-Nitride semiconductors makes this material system uniquely suited for fabrication of light emitting diodes peak emission wavelengths below 365 nm [12]. Figure 14 shows a schematic diagram of a typical AlGaN based LED.

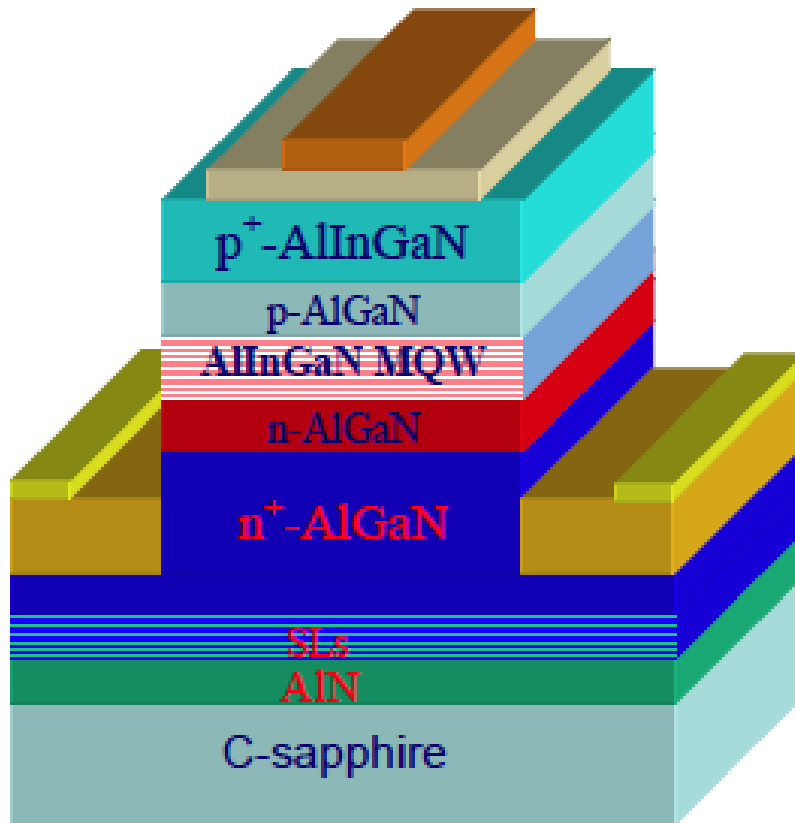


Figure 14. A schematic diagram of a typical AlGaN – based light emitting diode (From [12]).

The UVTOP[®] LEDs from SETI offer a viable option to serve as the light source for the IIFF patch. However, before a prototype UV patch could be developed it needed to be determined which LED wavelength and lens would best accomplish the purpose of the patch. Six different UVTOP models were purchased: LEDs with peak wavelengths of 255 nm and 270 nm for each of the three lens options. Measurements of the intensity and

the angular distribution of the intensity were performed for each model in an effort to find the optimum LED to serve as the light source for the device.

B. INTENSITY LOSSES

For line of sight imaging from the proposed device, high intensity at the detector is desired. This can be done by increasing the initial intensity of the light or decreasing the transmission losses that occur. As a beam of light travels away from its source, the optical power per cm^2 , or intensity of the beam will be affected by both geometric transmission losses, TL_g and transmission losses due to dissipation, TL_d . The overall intensity is given by Equation 5:

$$I(r) = I_0 [1 - TL_g(r)] [1 - TL_d(r)] \quad (5)$$

The dissipation losses are due to photon attenuation from either absorption or scattering reactions. Scattering reactions, which may prove useful for nonlinear of sight communications, will be covered in more detail in Chapter 5. The total dissipation loss due to both mechanisms is given by:

$$TL_d(r) = 1 - e^{-\alpha r} \quad (6)$$

The attenuation coefficient, α , is dependent upon the wavelength of the light and the properties of the medium through which it travels. Over the range of desired wavelengths, there is minimal change in the values of α . Also, for the UV IIFF device to function practically, it must be capable of working regardless of atmospheric conditions. In addition, under typical conditions the loss due to attenuation is negligible for distances less than 1 km [13]. For these reasons, transmission losses due to dissipation will not be addressed in this research.

The geometric losses are due to the divergence of the beam as it spreads out from the source. This is dependent upon the source's emission pattern and is different for each of the three types of LED lens. A broader emission pattern will have a higher geometric loss rate than a focused beam. However, despite the higher loss rate, the broader emission pattern could actually be beneficial in achieving the overall goal. In order to serve its purpose and identify a target as friendly, the device must emit a signal that is

seen by the engager. If the emitted beam were extremely narrow, the patch would have to be oriented such that the LED would be aimed directly at the engager. A broader emission pattern reduces the importance of the patch's orientation.

The objective becomes finding the ideal middle ground where there is a high intensity with the widest possible emission pattern at the range of interest. Therefore, both the intensity and emission patterns for each of the six types of purchased LEDs were measured. The results were then compared in order to choose the most effective model(s) of LED(s) to be used in the prototype device.

C. INITIAL INTENSITY MEASUREMENTS

In order to measure the intensity of the LEDs, a model FGAP71 GaP photodiode from Thorlabs was used. Photodiodes are able to convert energy received from incident photons directly into electrical current. The FGAP71 photodiode response has a wavelength range of 150-550 nm [14]. The responsivity of the photodiode is shown in Figure 15.

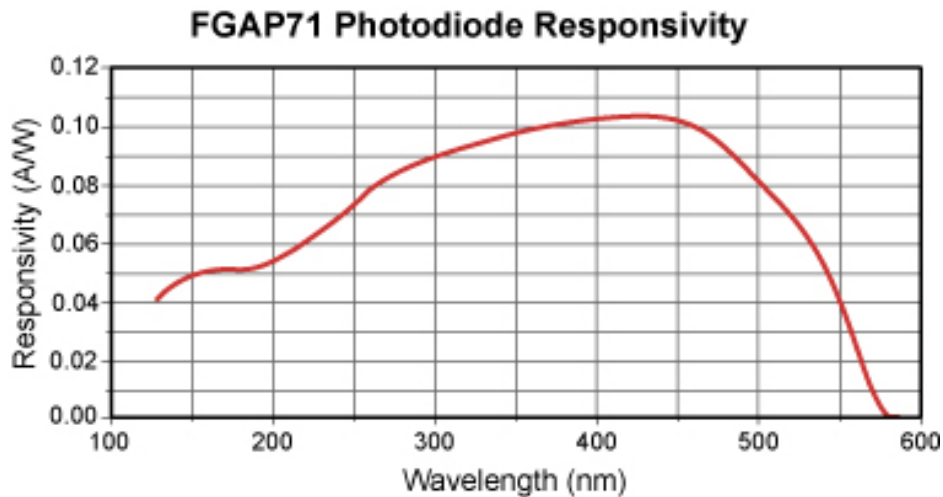


Figure 15. Responsivity of FGAP71 GaP Photodiode as a function of wavelength (From [14]).

The direct line of sight intensity of each of the six LED models was measured from a distance of 5 cm using the setup shown schematically in Figure 16. Each LED has a maximum rated value of 30 mA for a sustained forward DC current. Therefore, in each case the LED was driven at a constant current of 20 mA.

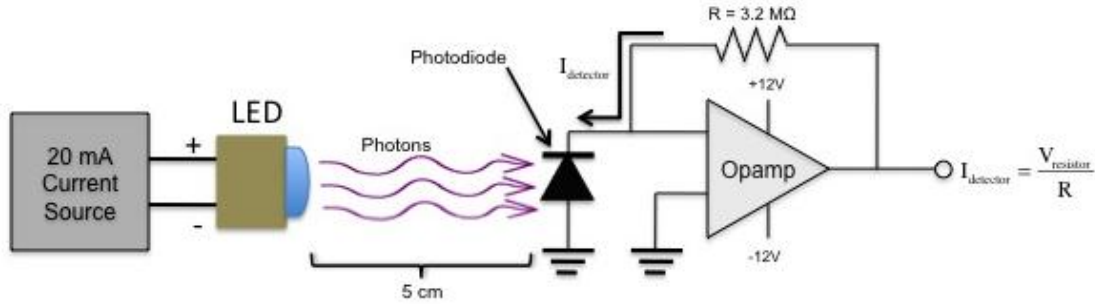


Figure 16. Setup used to measure intensity of various deep UV LED types.

The amount of light incident on the photodiode is directly proportional to the output current, I_{Detector} . By Ohm's law, the output current of the photodiode becomes:

$$I_{\text{Detector}} = \frac{V_{\text{Resistor}}}{R} \quad (7)$$

because the resistance is held constant, the voltage drop across the resistor is also proportional to the amount of light detected. This voltage was measured and recorded as a measurement of the optical power for each LED. The results are shown in Figure 17.

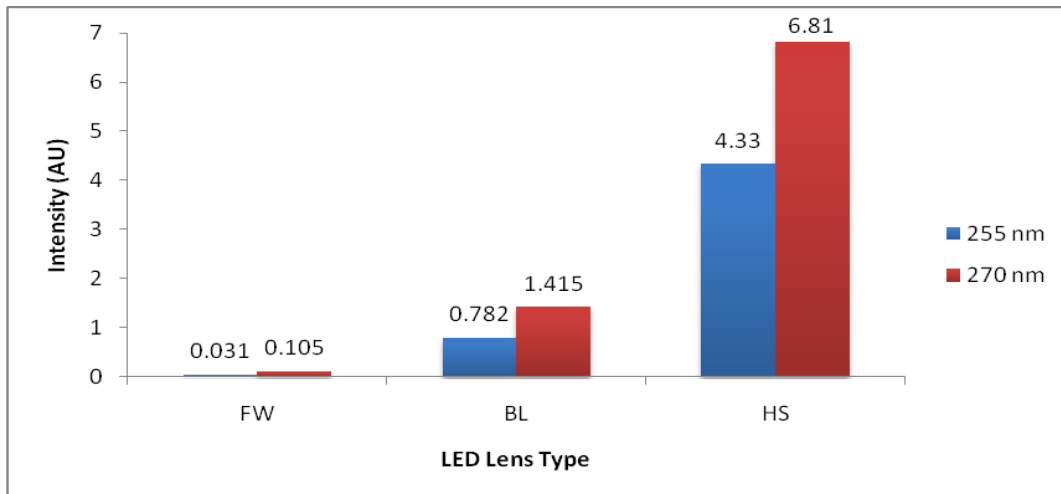


Figure 17. Measured intensities of LED models.

It is clear that the 270 HS LED is the brightest. It is more than 1.5 times brighter than the 255 model with the same window, and nearly 5 times brighter than any other model with the same peak wavelength. However, the HS LEDs also have the narrowest emission pattern. In order to determine which LED should be used, both parameters must be taken into consideration. However, Figure 17 also indicates that all 270 nm models are between 1.6-3.3 times brighter than the 255 nm models, while the emission patterns are the same. Therefore, only the 270 nm LEDs underwent further testing.

D. INTENSITY DISTRIBUTION MEASUREMENTS

Figure 18 shows the typical emission patterns corresponding to each type of LED lens as given by SETI.

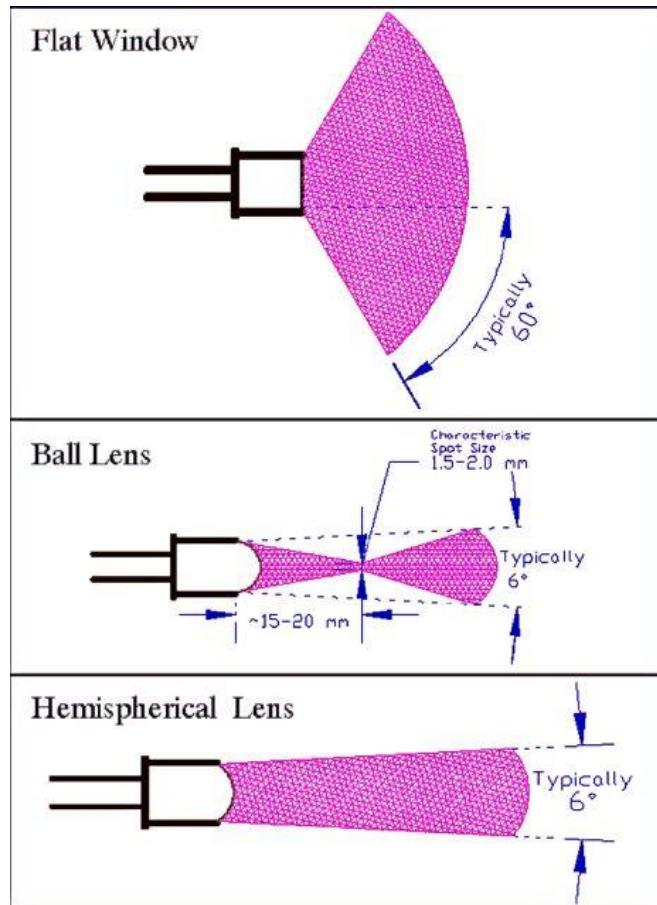


Figure 18. Emission patterns for UVTOP[®] LED lenses (From [15]).

Although these emission patterns provide a general idea of the angular dependence of the intensity, they give no indication of the intensity distribution within the cone. To obtain this information, a more precise measure of intensity as a function of emission angle was desired. This was accomplished using the same GaP photodiode arrangement that was used to measure the direct intensity. To measure the angular dependence of the intensity, the orientation of the LED was varied from 0° to 45° in 2° increments as shown in Figure 19.

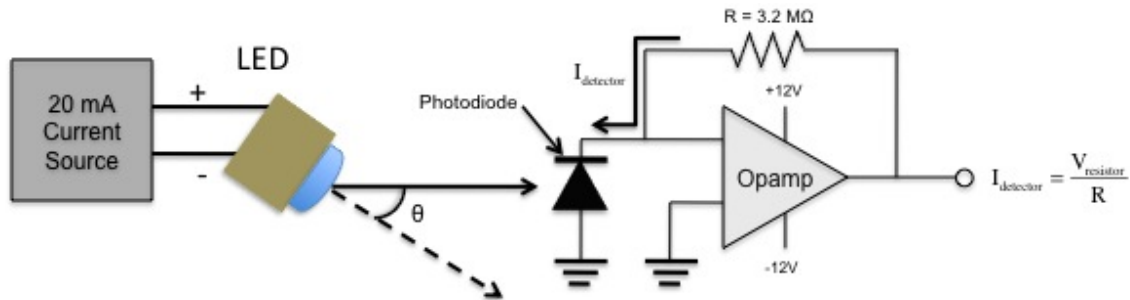


Figure 19. Setup used to measure angular dependence of intensity.

The same measurement was performed for each of the three lens types using 270 nm LEDs. Figure 20 shows a comparison of normalized intensity as a function of angle for all three lens types.

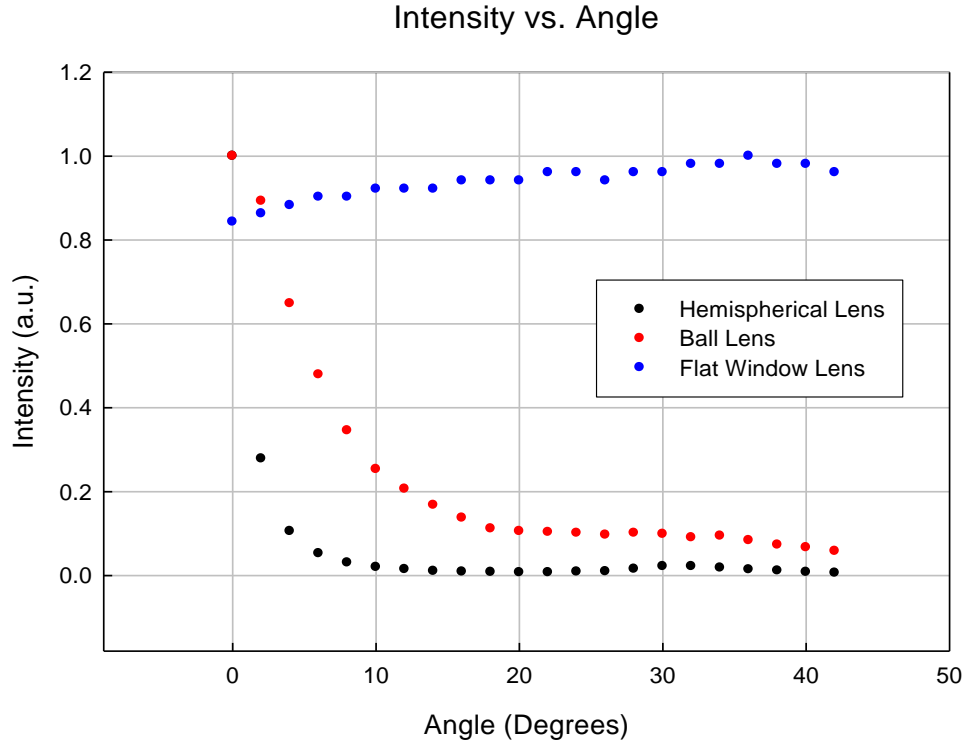


Figure 20. Normalized intensity as a function of LED angle. Initial point for hemispherical lens and ball lens LEDs overlap.

As expected, the intensity of the HS LED decreases the most quickly as the angle or orientation increases while the intensity of the FW LED remains fairly constant over the full range $\sim 40^\circ$ and actually reaches a maximum at $\theta = 36^\circ$. The BL LED however produces a broader emission pattern than expected. Although the HS LED is nearly 5 times brighter than the BL LED when $\theta = 0^\circ$, the BL model becomes more intense than the HS model when $\theta > 6^\circ$. However, because θ represents the half angle of the emitted beam, the HS LED remains the brightest for a total divergence of 12° . The FW LED is the brightest for $\theta > 22^\circ$.

E. EVALUATION OF 270 NM HS LED

The goal of this research was to develop a UV IIFF signaling device that could be viewed at up to 1 km during either day or night. To develop a functioning IIFF patch, a mobile UV source needed to be constructed and tested. Despite the narrow emission

pattern of the 270 nm HS LED, it was selected as the light source for the first mobile device. The goal of this device was to give an indication of both the day and night range of a single LED. The electronic circuit used to drive the LED is shown in Figure 21.

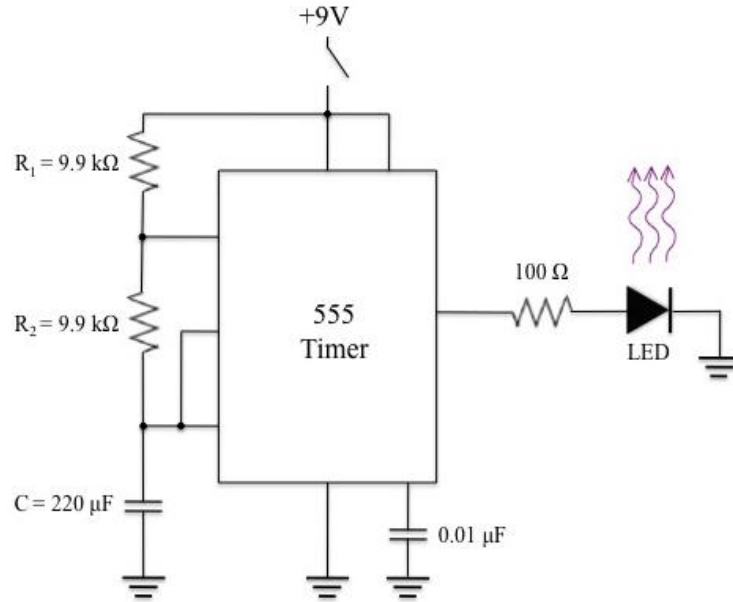


Figure 21. Circuit diagram of first mobile test device.

The LED was powered by a 9 V battery, and modulated with a 555-timing chip. By using a 555 timing chip, the amount of time that the LED is on, t_{hi} , and off, t_{low} , are given by:

$$\begin{aligned} t_{hi} &= \ln 2 \cdot (R_1 + R_2) \cdot C \\ t_{low} &= \ln 2 \cdot R_2 \cdot C \end{aligned} \quad (8)$$

Using values of 9.9 kΩ for each R_1 and R_2 , as well as 220 μF for C gave values of 3 seconds for t_{hi} , and 1.5 seconds for t_{low} . The initial choice for these times was driven by the nature of the data acquisition for the intensified PentaMAX camera. The 100 Ω resistor in series with the LED was chosen to produce a driving current of ≈ 20 mA.

Using this mobile device, images were taken during both day and night using the intensified PentaMAX camera described in chapter 2. Because the camera has a range of 180-800 nm and is sensitive to both visible and IR light, optical filters needed to be used to create the zero background condition. During the night there is significantly less

visible and IR light and the 270B filter alone was sufficient to create the desired condition. Using this filter only reduces the intensity of the source to 43% of the nonfiltered value. However, to capture images during the day, use of both the 270B and 270N filters still allowed significant levels of visible light to reach the camera. Although the transmission at any one point outside the bandwidth may be low (e.g. 10^{-6} - 10^{-8}) the integration over such a wide background wavelength range is not negligible. In addition, the use of both filters reduces the intensity of the source to less than 10%. Because of this, the device was seen at significantly further ranges during the night versus day.

During the day, the maximum range for which the device was discernable was ~ 100 m. A daytime image of the device with 50 ms exposure at 100m is shown in Figure 22.



Figure 22. Daytime image of single 270 nm HS LED with 20 mA driving current viewed from 100 m through 270N and 270B solar blind filters with 50 ms integration time.

Notice that due to the intensity of visible light present, the outline of the background is present in the image. The background appears out of focus because the UV light and visible light refract differently when passing the lens of the camera. Therefore, the lens can bring either the visible or the UV light into focus, but not both simultaneously.

At night, the device was visible at 300 m; it was not tested at ranges beyond this. Figure 23 compares images captured at night at distances of 100m and 300m.

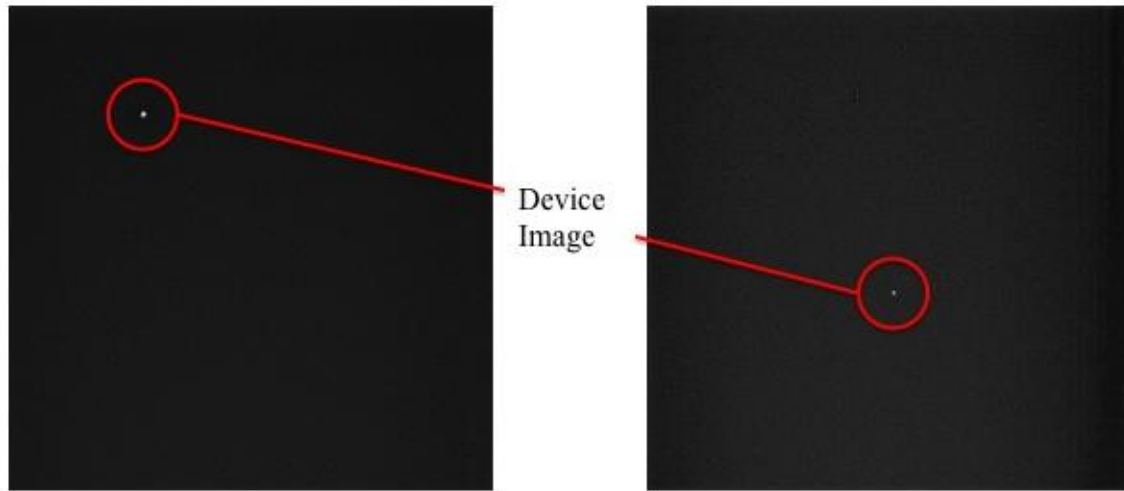


Figure 23. Nighttime images of single 270 nm HS LED with 20 mA driving current. Left: Viewed from 100 m through 270B solar blind filter with 20 ms exposure time. Right: Viewed from 300 m through 270B solar blind filter with 100 ms exposure time.

The Winview software creating the image assigns the color white to the pixels with the highest photon counts, regardless of the actual value. The other pixels are then assigned various shades of gray, or even black based upon their relative photon counts. This makes it impossible to judge the actual intensity of the light received from the device merely by looking at the image displayed. However, the counts received by each pixel are recorded as long as the count does not exceed the saturation point of 4095.

Figure 24 shows the same images as plotted by MATLAB using a program that reads the photon count of each pixel once the image has been stored as a TIFF file.

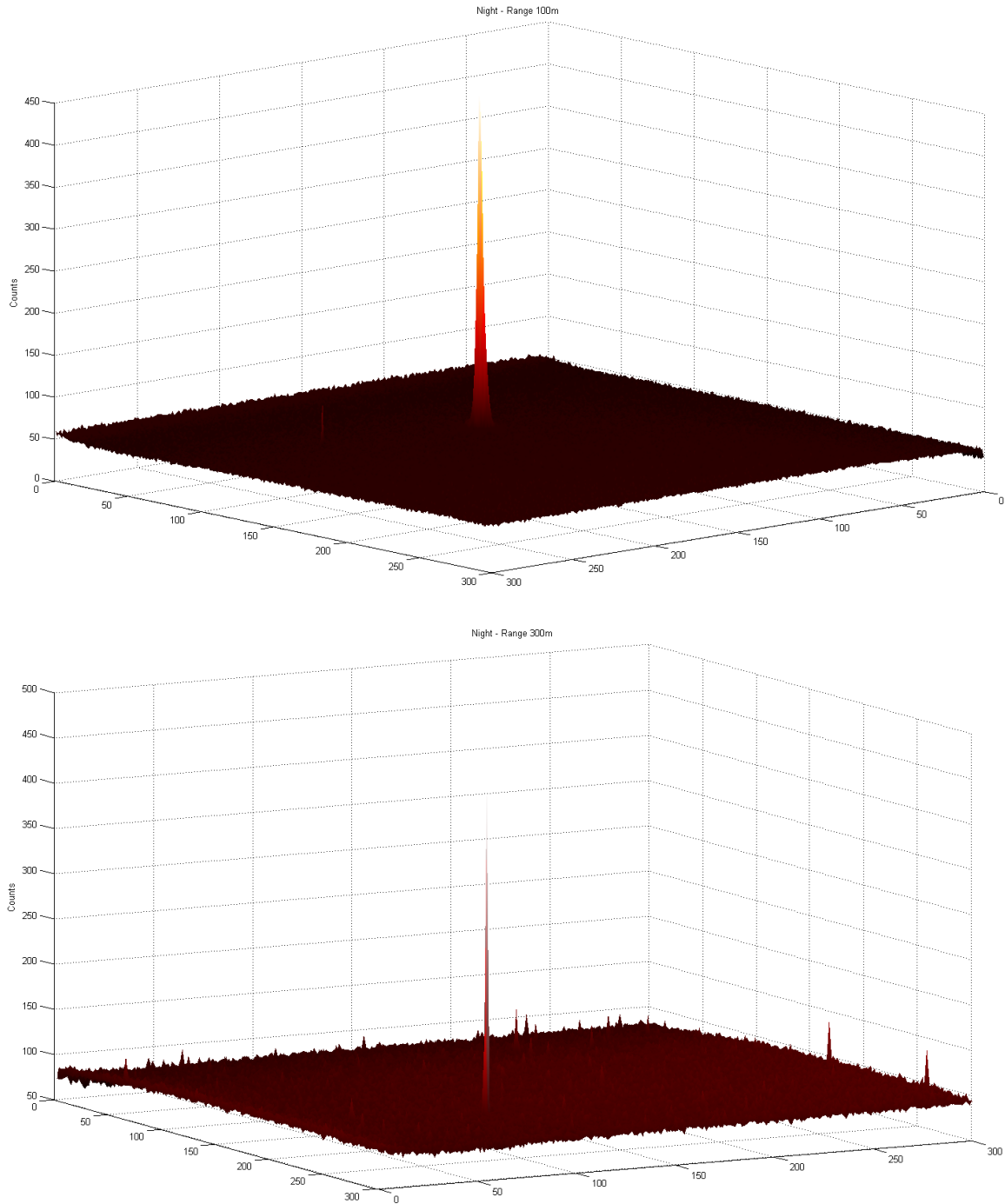


Figure 24. MATLAB plots of images from Figure 9. Top: 270 nm HS LED with 20 mA driving current viewed from 100 m with 20 ms exposure time. Bottom: 270 nm HS LED with 20 mA driving current viewed from 300 m with 100 ms exposure time.

By importing the data from the TIFF file, MATLAB is also able to easily find the maximum photon count received by any pixel in the ccd array. At a range of 100 m the maximum count was 450, compared to a maximum count of 454 received at 300 m. However, the camera was exposed for 100 ms at 300 m as compared to only 20 ms at 100 m.

F. SUMMARY

UVTOP[®] LEDs from the Sensor Electronic Technology Corporation offer the best chance of serving as the light source of a potential solar blind UV IIFF patch. The 270 HS LED provides a significantly higher intensity than other models tested, and a single 270 HS LED with a 20 mA driving current was shown to be visible at ranges of 100 m during the day and 300 m at night. To produce a prototype IIFF patch visible at up to 1 km both day and night, more light will need to be emitted from the source. Further experiments conducted and presented in Chapter 4 will address the possibilities of using a device with multiple LEDs, each with higher driving current, to scale the output for the desired performance range.

THIS PAGE INTENTIONALLY LEFT BLANK

IV. LED PERFORMANCE OUTSIDE RECOMMENDED OPERATING PARAMETERS

A. RECOMMENDED OPERATING PARAMETERS

It is clear from the results of the previous chapter that in for the proposed device to be effective at distances of up to 1 km, more light needs to be detected. Either improving the efficiency of the filters and/or detector or emitting more light from the transceiver can achieve this. The quickest and easiest solution is to produce more light. There are two ways this can be accomplished using the UVTOP[®] LEDs: using multiple LEDs or increasing the luminosity of the LED by increasing the driving current. The research presented in this chapter was done with the purpose of finding the optimal current with which to drive the LEDs.

According to the specifications from SETI, each of the UVTOP[®] 270 nm series LEDs is rated for a maximum sustained forward DC current of only 30 mA and a peak forward current of 200 mA (duty factor = 1%, frequency = 1 KHz) [15]. The UV IIFF/signaling application requires an intermediate case of pulsed operation at low frequency (e.g. 1-10 Hz). In order to find the ideal current that would produce the maximum possible output power, each type of LED was tested to see how they would behave with increased driving voltage and current. The results of these experiments were analyzed and used to design a second mobile test device containing multiple LEDs with higher intensities.

B. CURRENT MEASUREMENTS AS A FUNCTION OF BIAS VOLTAGE

To understand the behavior of the LEDs at higher driving currents, the current and intensity were measured for increased values of bias voltage. Using the 270 nm model LEDs, the forward voltage was increased from 0 V to 8.4 V in increments of 0.2 V. At each voltage, the forward current through the LED and the UV intensity were measured. As the current rose above 30 mA, the voltage was applied only for the time needed to

take the measurement. The measurements were performed for three separate FW LEDs, two BL LEDs, and four HS LEDs, and the resulting currents were averaged for LEDs of the same lens type. Figure 25 shows the measured currents plotted against the corresponding driving voltages.

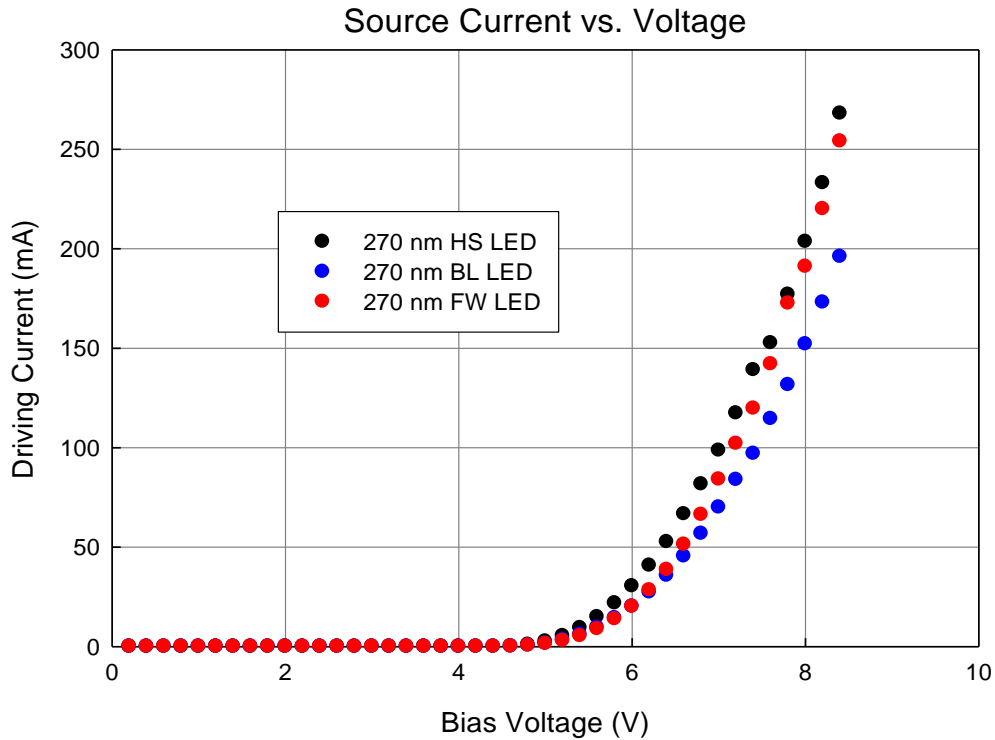


Figure 25. Current as a function of bias voltage for 270 nm LEDs of each lens type.

While there were slight variations amongst samples of the same lens type, these variations were small. However, the differences are more pronounced between LEDs of different lens types. For a given voltage, the average current through the HS LEDs is as much as 40% higher than the average for the BL LEDs.

Because LEDs depend upon recombination of injected carriers for the emission of photons, the amount of light produced is dependent upon the forward current and not the forward voltage. However, the power (P) consumed in each case is given by $P=IV$. Therefore because the HS model LED has the highest current for any given voltage, use of this model allows for either higher optical output for the desired power consumption or

lower power consumption for the desired optical output. This is a significant advantage of the HS LED considering it is also the brightest of the three models.

C. INTENSITY MEASUREMENTS AS A FUNCTION OF CURRENT

In addition to the forward current, the intensity of the emitted light was also measured for each driving voltage. As before, this was done with a GaP photodiode using the setup shown in Figure 26.

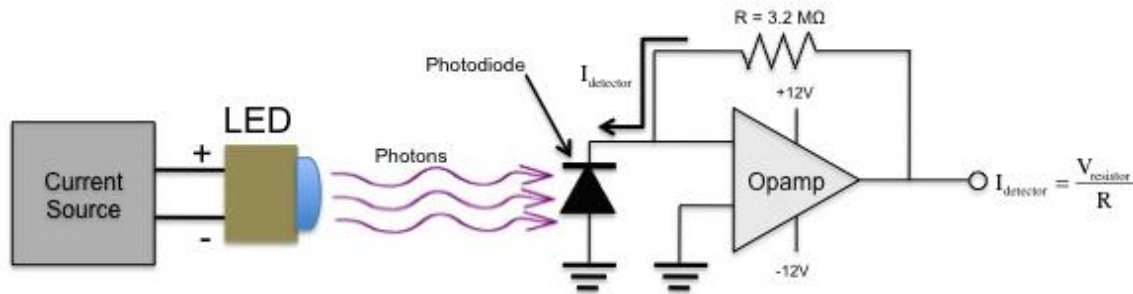


Figure 26. Setup used to measure intensity as a function of current.

Due to the large difference in intensity between the LEDs of different lens types, the distance from the LED to the photodiode was not held constant. To avoid the output voltage limit on the opamp, the intensity of the four HS LEDs was measured at a distance of $\sim 15\text{cm}$. For the sake of comparison, the intensity of the two BL LEDs was measured at the same distance. In order to provide significant signal strength, the intensity of the three FW LEDs was measured at a distance of only $\sim 5 \text{ cm}$. Figure 27 shows the resulting intensities as a function of driving current for the HS models.

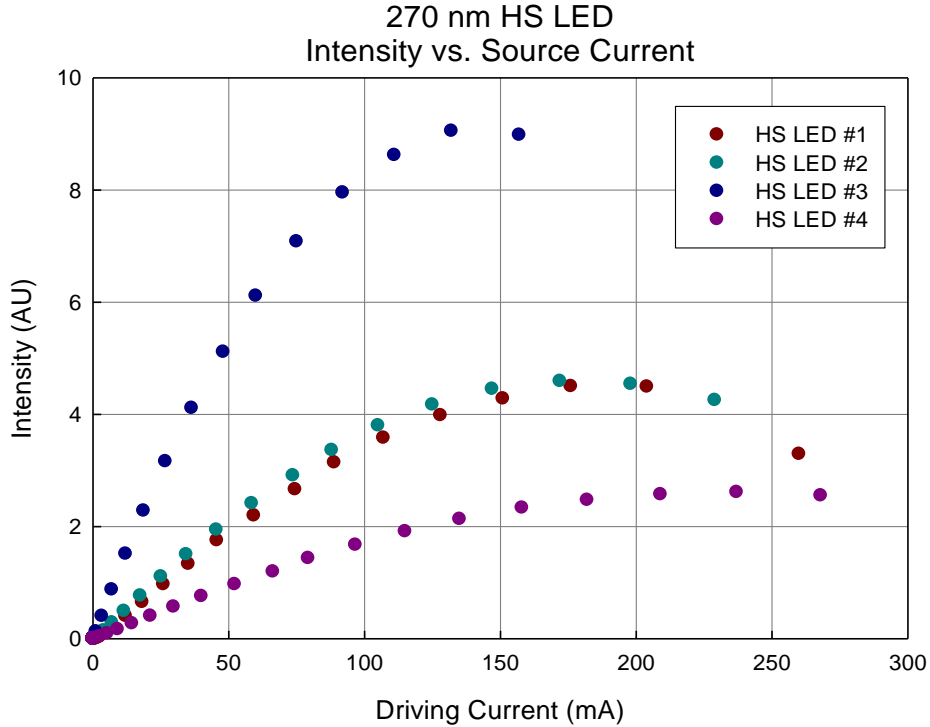


Figure 27. Intensity as a function of current for 270 nm HS LED.

Unlike the forward current, the intensities of the LEDs varied significantly between the samples. The LEDs referred to as #1 and #2 were in fairly good agreement; the light of sample #3 was more than double the intensity, and sample #4 only half the intensity of #1 and #2. This disparity is attributed to the LEDs still being in the research state of their development with significant variations in material quality. As the technology and production capacity advance it is expected that the intensity will be more consistent among LEDs of the same model.

As expected, at low current the intensity of the LEDs increases linearly with current. However, at higher currents, the relationship is sublinear and eventually increasing the current actually causes the intensity to decrease, probably due to heating effects. The maximum intensity for each is roughly 5 times higher than the intensity corresponding to a current of 20 mA, which was the current used in the first mobile test

device. Using LED #3 as the limiting case, an upper limit of ~150 mA can be placed upon the desired forward current, as values above this provide no additional optical power.

Although the experiments of the previous chapter clearly established the HS model as the brightest, both the BL and FW models offer a more dispersed emission pattern. Because of this advantage, before eliminating these models as candidates for the IIFF patch, the intensities of these models were measured at higher currents. This was done in order to determine if a sufficient driving current existed for which either model could produce necessary power to be seen at the desired ranges. Figure 28 shows the intensity of each of the BL LEDs as a function of the driving current.

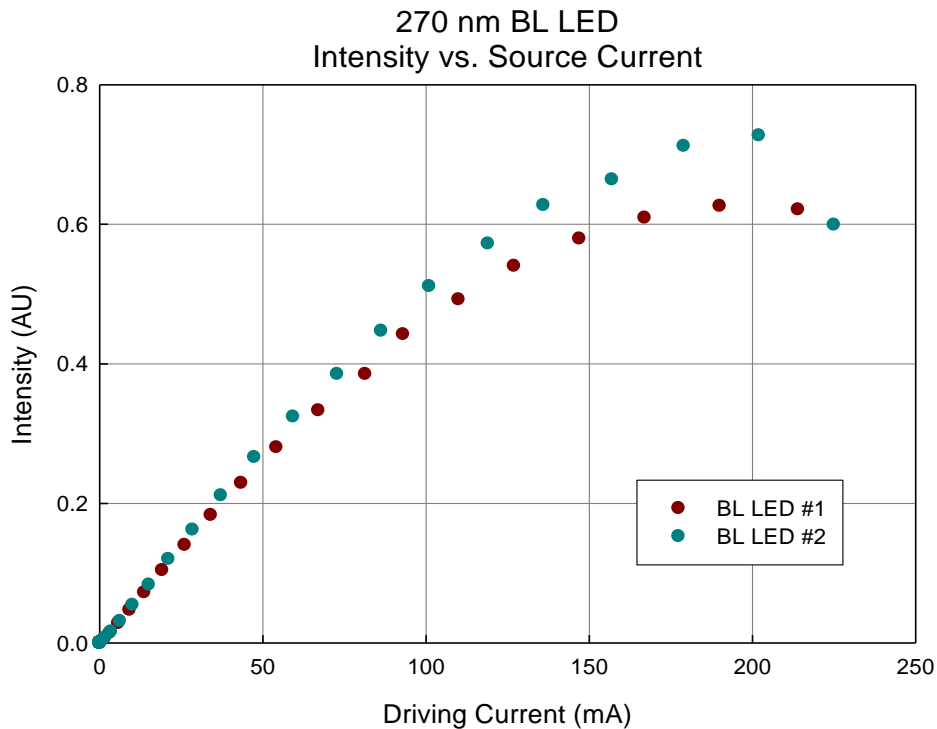


Figure 28. Intensity as a function of current for 270 nm BL LED.

The maximum intensity for each BL sample was achieved at currents of ~ 200 mA. Because the BL LEDs were tested at the same distance as the HS LEDs, a direct comparison between the intensities of the two models can be made. The maximum intensity of the BL models corresponds to the intensity of an HS LED being driven at

only 20 mA, the same current used in the first mobile test device. This intensity would allow one BL LED to be visible at distances of 100 m during the day and 300 m at night. To achieve ranges up to 1 km, the number of LEDs needed would significantly increase the demand on the power supply and increase the size of the IIFF patch. While these results do not eliminate the BL model from future consideration, optimization of the HS model was the focus of further experiments.

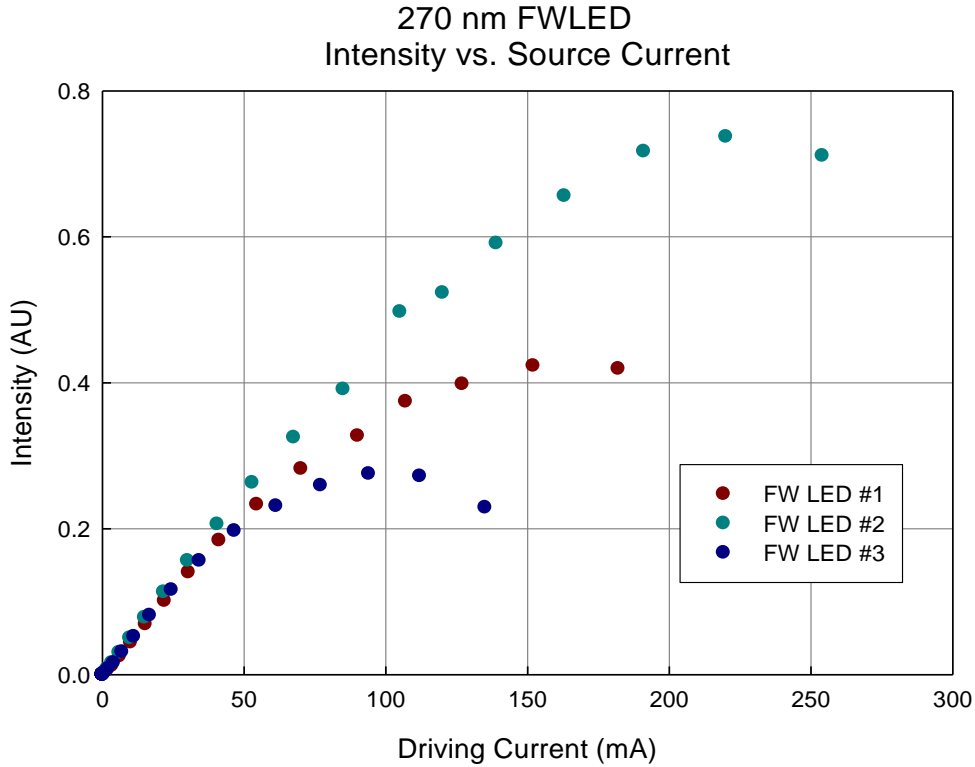


Figure 29. Intensity as a function of current for 270 nm FW LED.

Finally, Figure 29 shows the measured intensity of each of the FW LEDs as a function of driving current. As with the HS samples, the intensity between the FW samples varied significantly, especially at currents above 50 mA. The brightest of the FW samples, #2, approached an intensity of only 0.8 V. Although the intensity produced by the FW LEDs is approximately the same intensity produced by the BL samples, recall that FW measurements were taken from a distance of only 5 cm whereas the BL and HS measurements were performed from a distance of 15 cm. Despite the advantage of the

wide emission pattern of the FW LEDs, using them to produce the desired intensity would require the use of significantly more LEDs and increase the size, cost, and power consumption of the resulting device. Hence, it was concluded that the UVTOP[®] FW LEDs would not be a possible source for a solar blind IIFF device.

D. TRANSIENT INTENSITY MEASUREMENTS

While conducting the experiments measuring the intensity of the LEDs at increasing voltages, it was noticed that at high currents, the intensity began to decrease with time. This decrease in intensity is attributed to an increase in LED temperature at excessive currents. As shown in Figure 30, the output power of the LED decreases with a rise in temperature.

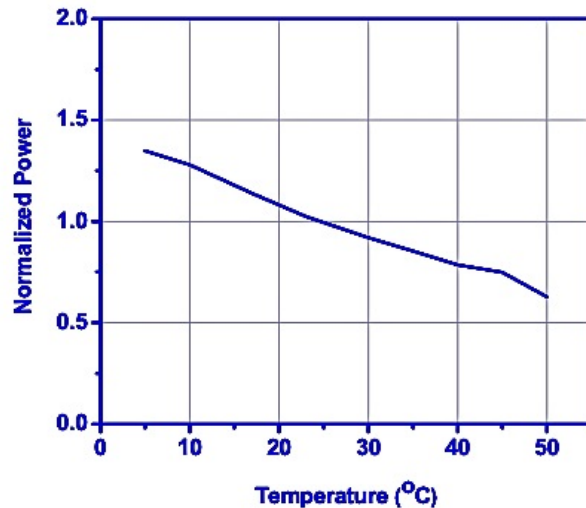


Figure 30. Normalized power as a function of temperature for UVTOP[®] 270 nm LEDs. Normalized power = 1.0 at 25°C (From [15]).

At low currents, the LED is able to dissipate heat at the rate it is produced; this should cause the temperature to remain constant and the intensity to also be constant with time. However, as the current increases, the LED reaches a point when the heat can no longer be dissipated at an equivalent rate and the device temperature begins to rise. As the temperature rises, less power is emitted from the LED reducing the range at which it can be detected.

To measure the effect of increasing temperature, the intensity of a HS LED was measured over a 35-40 second period for driving voltages up to 8.0 volts. As before, a GaP photodiode was used in conjunction with an opamp, but the output voltage was read with an oscilloscope rather than a voltmeter. Figure 31 shows the setup used.

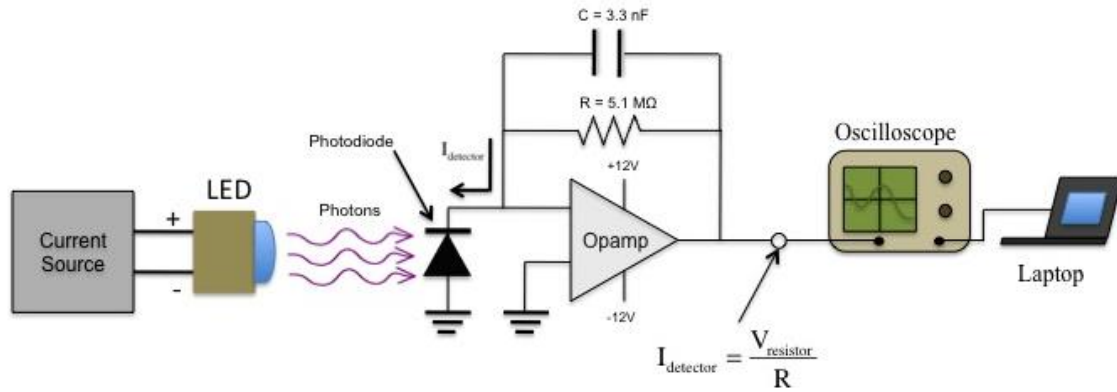


Figure 31. Setup used to measure LED intensity as a function of time.

The time scale on the oscilloscope was set to 5 seconds per division, giving a total display time of 40 seconds. A Labview program recorded voltage and time values from the oscilloscope and stored them in text format on a computer. Figure 32 shows how the intensity behaves with time with increasing values of driving voltage.

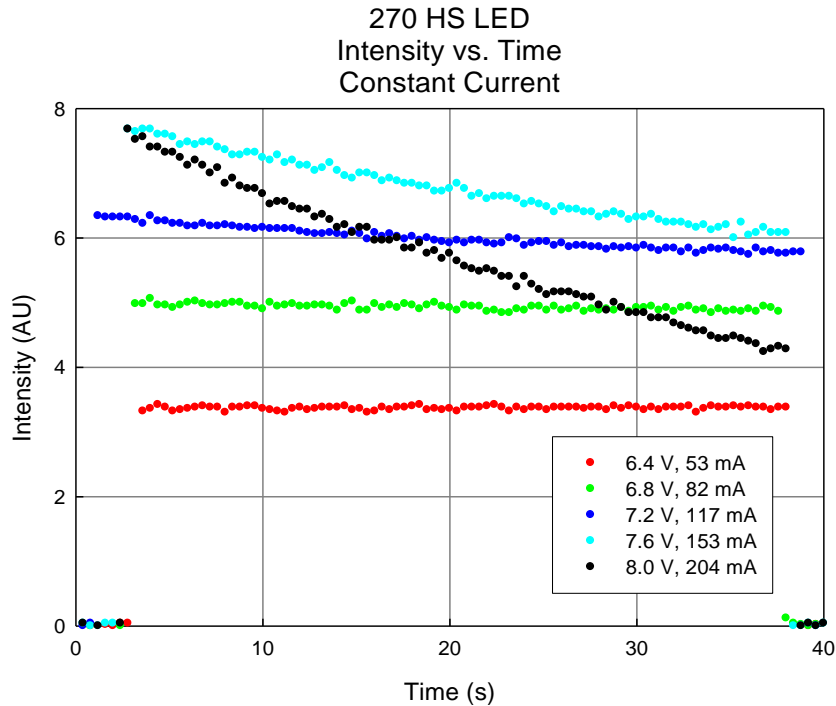


Figure 32. Intensity as a function of time for 270 nm HS LED at constant current.

For a forward bias voltage of 6.4 V, which corresponds to a 53 mA driving current, the power output of the LED is constant for the entire time, but with an applied voltage of 6.8 V, the intensity does begin to drop slightly. The rate of power decrease becomes even more severe at higher voltages. As the forward current just exceeds 200 mA, the power drops to nearly half of the original value in less than 40 seconds. In addition, the initial intensity is equal to that achieved with a current of 150 mA.

In order to avoid overheating of the LEDs, either the rate of heat production must be decreased, or the rate of dissipation increased. The heat production rate can be controlled by limiting and/or pulsing the driving current. Through pulsing, it becomes possible to drive the LED at significantly higher currents for a brief interval, followed by a cooling period during which no current is applied. Both limiting the driving time and extending the cooling time can prevent the LED temperature from rising. In addition, a pulsed driving current is desired for an IIFF patch because a flashing light is more likely to be seen by the observer.

Figure 33 shows the intensity of a 277 nm LED as a function of wavelength for DC currents ≤ 50 mA, and 10 μ s current pulses ≥ 50 mA [12]. Note that the peak wavelength remains fairly constant for an 80x increase in driving current.

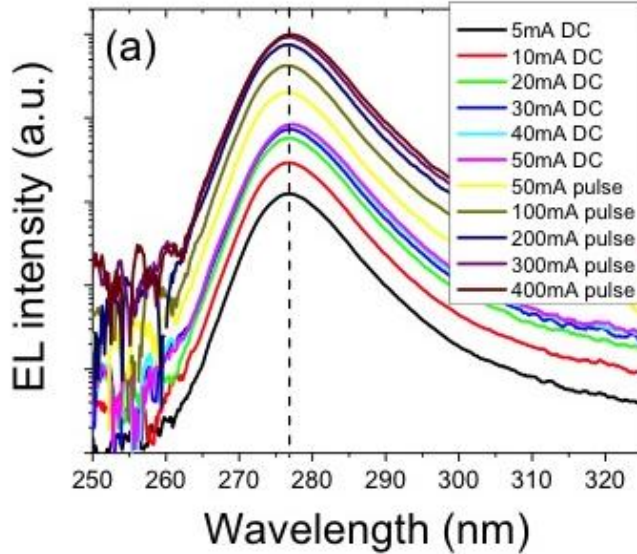


Figure 33. Electroluminescence spectra of 277 nm LEDs under different currents. For current ≥ 50 mA a 10 μ s pulse was used (From [12]).

Using this very brief pulse followed by a relatively long cooling time the maximum intensity is reached with a driving current of 400 mA. However, this intensity is only ~ 1.3 times higher than that achieved with a 200 mA current, and negligibly higher than that achieved with a 300 mA current. Also, in order to fulfill the purpose of the intended IIFF device as well as accommodate limitations on minimum detector exposure times during imaging data collection with the intensified PentaMAX camera, pulse durations longer than those allowing for maximum intensity are needed. The use of longer pulse times that is required for this research will limit the driving current to values significantly lower than the 400 mA seen in Figure 33.

Using the same setup shown in Figure 31, the intensity of the HS LED was measured at 40-second intervals for various pulse patterns. Figure 34 shows the intensity for a pulsed current with frequency = 5 Hz and a 50 % duty factor.

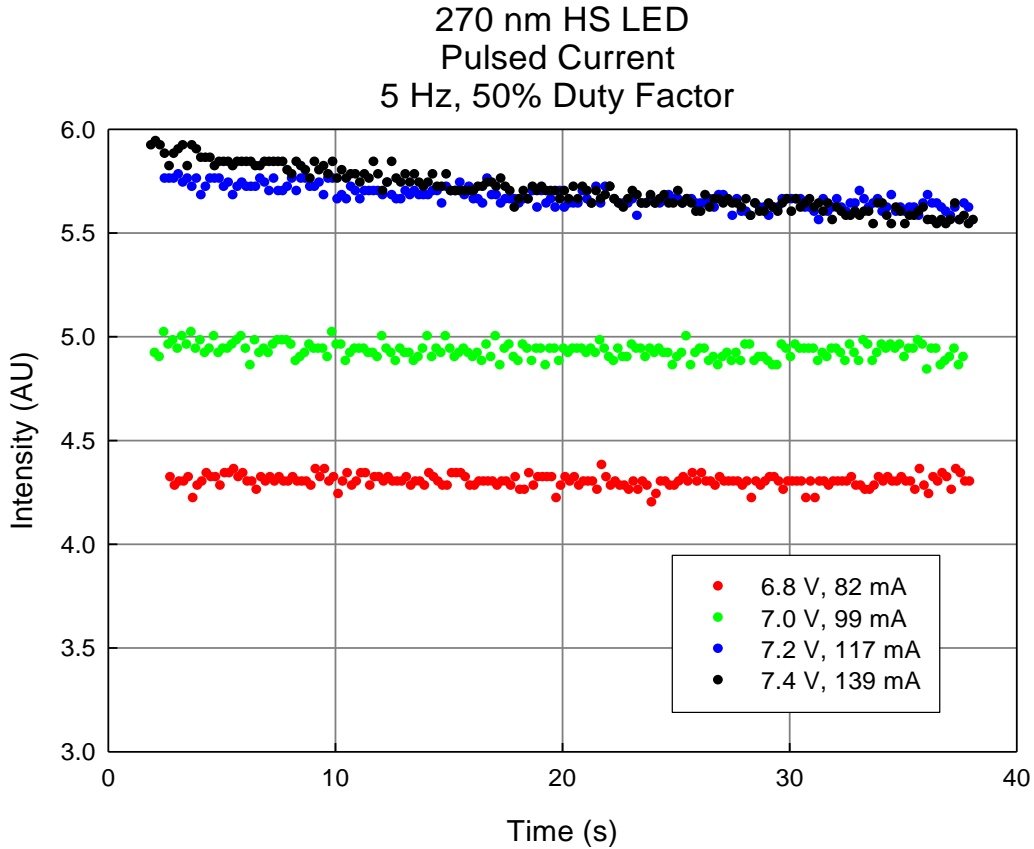


Figure 34. Intensity as a function of time for 270 nm HS LED pulsed current.

Notice that for this frequency and duty factor, the intensity does not begin to decrease with time until the driving current reaches roughly 120 mA. Under constant current conditions, this rate of intensity decrease was seen with a driving current of only 80 mA. Even though the duration of the pulse is 100 ms (10,000 times longer than the 10 μ s recommended pulse), it still allows for a 50% increase in driving current before significant effects of heating begin.

Figure 35 compares the decrease in intensity of an LED with a constant driving current of 120 mA with the decrease in intensity of the LED with two pulsed currents also at 120 mA. The first pulsed current had a 50% duty factor, delivering a 250 ms pulse followed by a 250 ms rest. The second pulsed current had a duty factor of 33%, delivering a pulse of 500 ms followed by a 1-second rest.

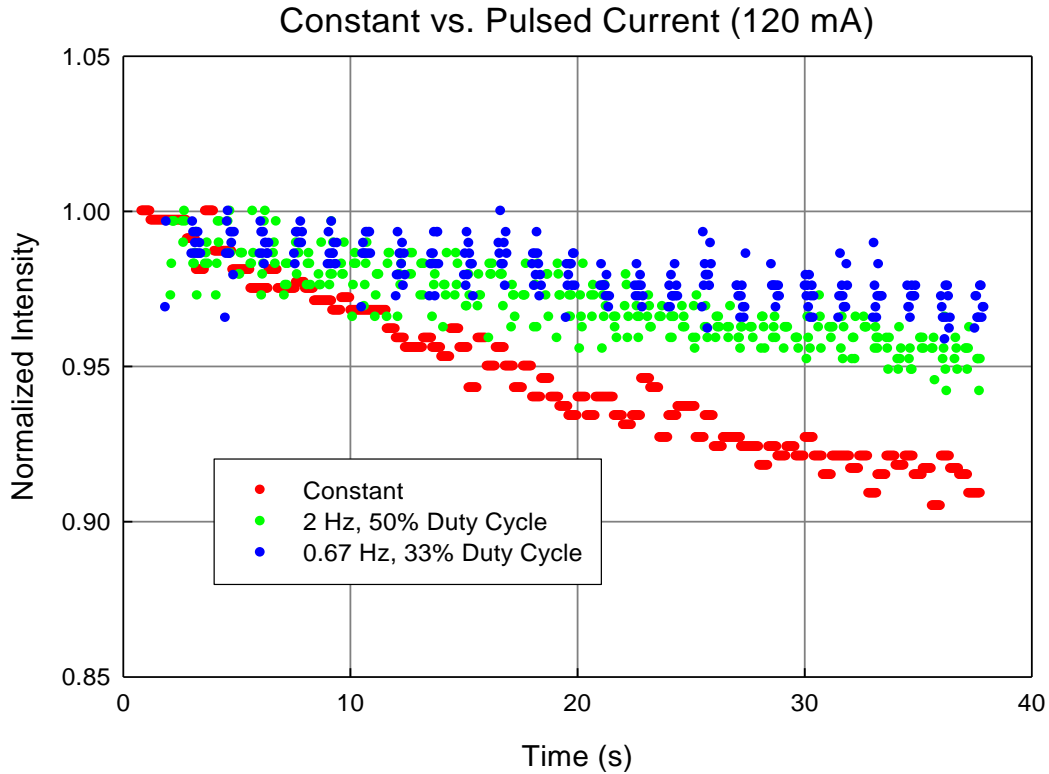


Figure 35. Comparing intensity as a function of time of 270 nm HS LED for 120 mA DC current vs. 120 mA pulsed current.

It is clear that by pulsing the current, the power output of the LED does not drop as fast. However, in comparing the power output of the pulsed LEDs, operation with the driving current at 0.67 Hz with a 33% duty cycle has the smaller rate of intensity drop. Even though the duration of the pulse is double that of the other current, the extra time between pulses allows the LED to cool more, resulting in a smaller drop in intensity over time.

E. EVALUATION OF PERFORMANCE FOR OPERATION OUTSIDE OF RECOMMENDED OPERATING PARAMETERS

Using the information from the experiments presented in this chapter, a second mobile test device was designed. In consideration of the eventual constraints on the size and power supply of a solar blind UV IIFF patch, the device used four 270 nm HS LEDs. The driving current was set at 70 mA. This allows each LED to produce more than 3

times the power output of the LED used in the first mobile device. In addition, even though the device would be used for minutes at a time during testing, 70 mA falls well below the lower limit at which the samples showed signs of heating. Figure 36 shows the circuit used in the construction of the device.

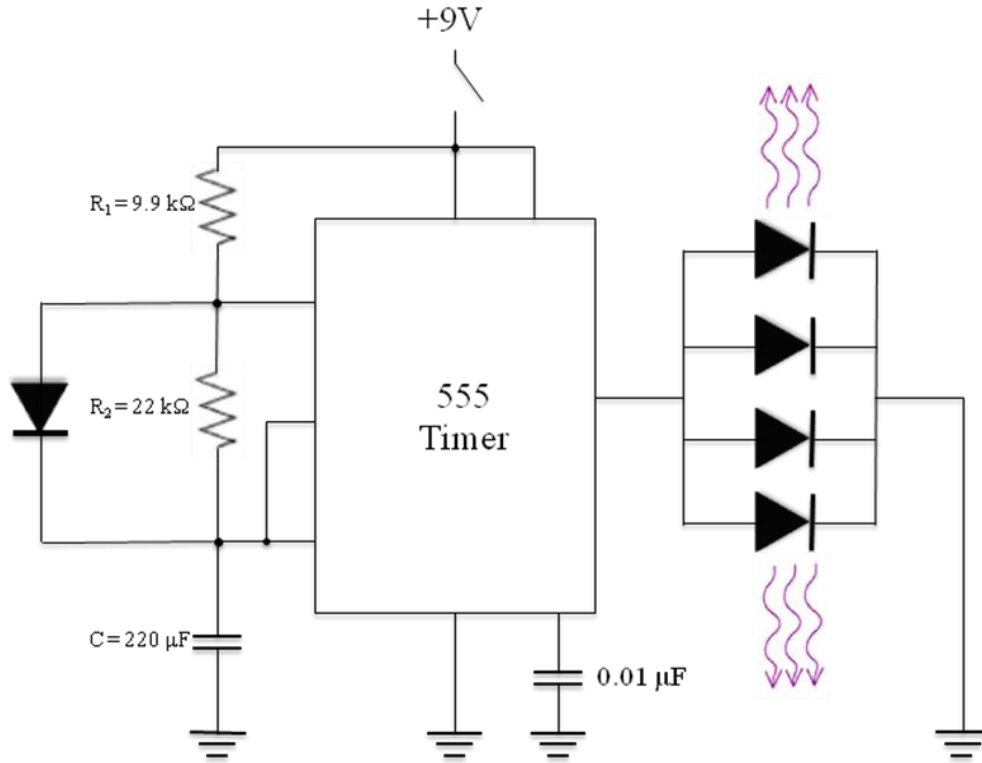


Figure 36. Circuit diagram of second mobile test device.

As with the first test device board, a 555 timer was used to create the pulsed driving current. The use of a diode parallel with R_2 changes the equations for t_{hi} and t_{low} to:

$$\begin{aligned} t_{hi} &= \ln 2 \cdot R_1 \cdot C \\ t_{low} &= \ln 2 \cdot R_2 \cdot C \end{aligned} \quad (9)$$

This allows for a duty cycle of less than 50%. Using values of 9.9 kΩ for R_1 , 22 kΩ for R_2 , and 220 μF for C resulted in a pulsed current with a frequency of 0.22 Hz and a duty factor of 33%. The 1.5-second pulse was designed to provide sufficient exposure time for the intensified PentaMAX camera.

Images of the device were taken during both the day and night using the intensified PentaMAX camera. During both day and night, the test device was clearly visible at a range of 300 m. However, due to the absence of longer line of sight range, the device was not tested beyond this distance. Figure 37 is an image of the device viewed at 300 m during the day with a 150 ms exposure time using both the 270N and 270B optical filters. The maximum daytime pixel count recorded for a 150 ms exposure at this distance was 1016 counts.



Figure 37. Daytime image of four 270 nm HS LEDs each with 70 mA driving current viewed from 300 m through 270N and 270B solar blind filters with 150 ms exposure time.

Figure 38 is an image of the device viewed at 300 m during the night with a 15 ms exposure time using only the 270B optical filter. The maximum nighttime pixel count recorded for a 150 ms exposure at this distance was 4095 counts, indicating that some pixels of the ccd became saturated.

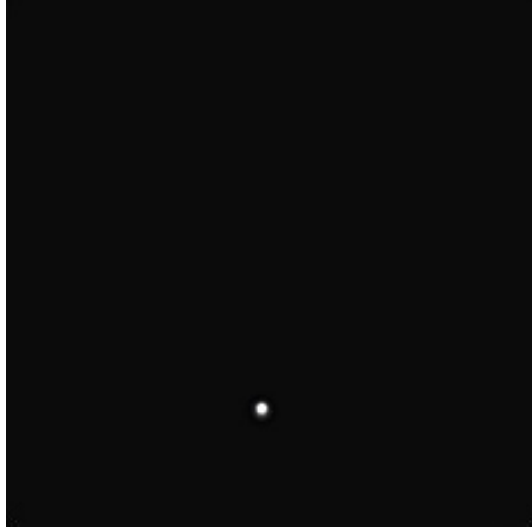


Figure 38. Nighttime image of four 270 nm HS LEDs each with 70 mA driving current viewed from 300 m through 270B solar blind filter with 150 ms exposure time.

F. SUMMARY

In order to produce a prototype solar blind UV IIFF device visible at distances up to 1 km during both day and night, each LED needs to be driven at the optimal current for this particular application. By measuring the behavior of the intensity and the current with increasing voltages, it was determined that utilizing a pulsed current would safely allow each LED to be driven at 70 mA for extended periods of time, even though this exceeds the recommended maximum operating current. A device using four 270 nm HS LEDs each operating at this current was clearly viewed both day and night from a distance of 300 m. It was not tested at longer ranges.

THIS PAGE INTENTIONALLY LEFT BLANK

V. SCATTERING AND NONLINE OF SIGHT DETECTION

A. RAYLEIGH SCATTERING

As light propagates through a medium, such as air, it interacts with the medium through absorption and scattering. Scattering reactions can cause a photon to change its direction of propagation, which can allow for detection of light even when the source is not in the line of sight of the detector. An example of this is shown in Figure 39, which is an image of a 270 nm HS LED directed to the right scattering off of chalk dust in the air and being imaged by the intensified PentaMAX camera placed at a 90° angle to the source.

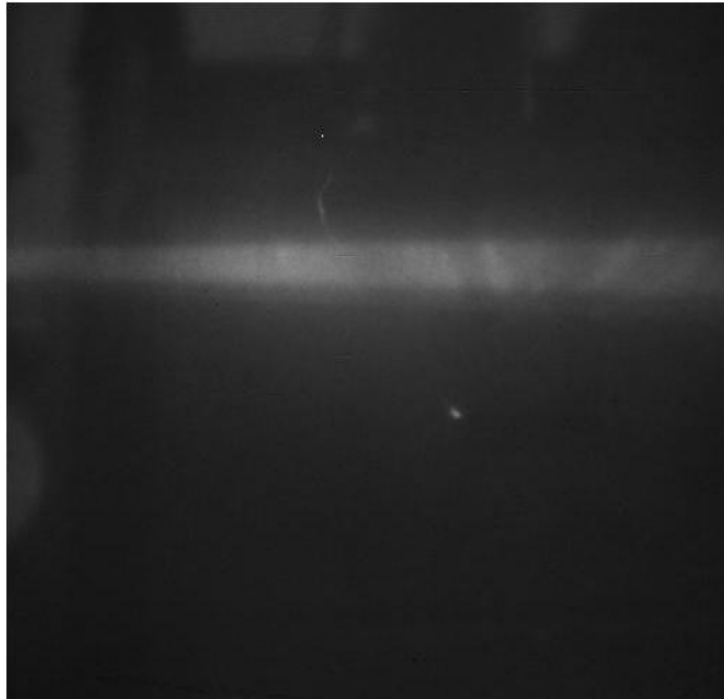


Figure 39. Example of NLOS imaging. UV light being scattered through chalk dust.

Of particular interest to the solar blind UV IIFF patch project is Rayleigh scattering, which refers to the scattering of light from particles up to about a tenth of the wavelength of the light. One example of Rayleigh scattering is the scattering of light off

of the bound electrons in the molecules of the air. In the late nineteenth century, Rayleigh derived the cross section for this reaction as:

$$\sigma = \frac{32\pi^3}{3\lambda^4 N} (n-1)^2 \quad (10)$$

N is the number of scattering particles per unit volume, n is the index of refraction, and λ is the wavelength of the incident light [16].

That the cross section varies as $1/\lambda^4$ indicates that the probability that an incident photon will undergo this type of scattering greatly increases at shorter wavelengths. Because the wavelength of the photons emitted by 270 HS LEDs is only half the wavelength of green light, these UV photons are 16 times more likely to undergo Rayleigh scattering when traveling through air. One goal of this research is to explore the possibility of utilizing this increased probability for scattering to perform NLOS detection in air. The capability for NLOS detection could allow the source to be seen even if blocked by buildings, vegetation, hills, or other obstacles (Figure 40).

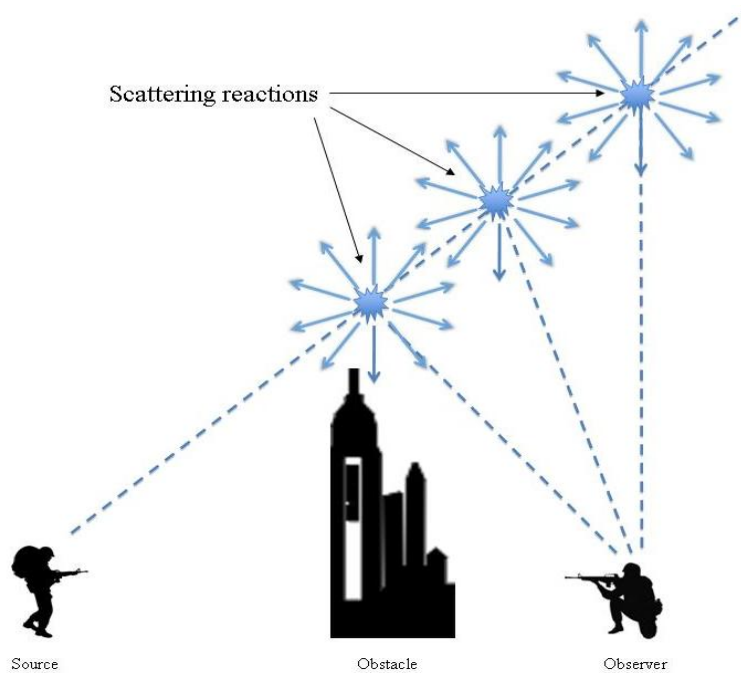


Figure 40. Due to the higher rate of scattering for UV light, it may be possible to perform NLOS detection or signaling. Scattering reactions in the air send photons in all directions. Some of these will propagate toward the observer, providing a means of visual communication even if the direct path is blocked.

B. NLOS DETECTION USING LOCK-IN TECHNIQUES

Using photomultiplier tubes (PMTs) as detectors, research efforts have been made to detect the scattering of photons in the solar blind region. Because of the high gain provided by the use of PMTs, the scattering of photons from molecules in the air has been detected with separation distances between source and receiver in the 10's of meters. The results of these experiments show promise toward developing channels of NLOS communication for both military and civilian applications [10, 13].

Using a FGAP71 GaP photodiode, attempts were made in our laboratory to measure the intensity of scattered UV light from a single HS 270 nm LED with a 60 mA constant driving current. Figure 41 shows the experimental setup used in these efforts.

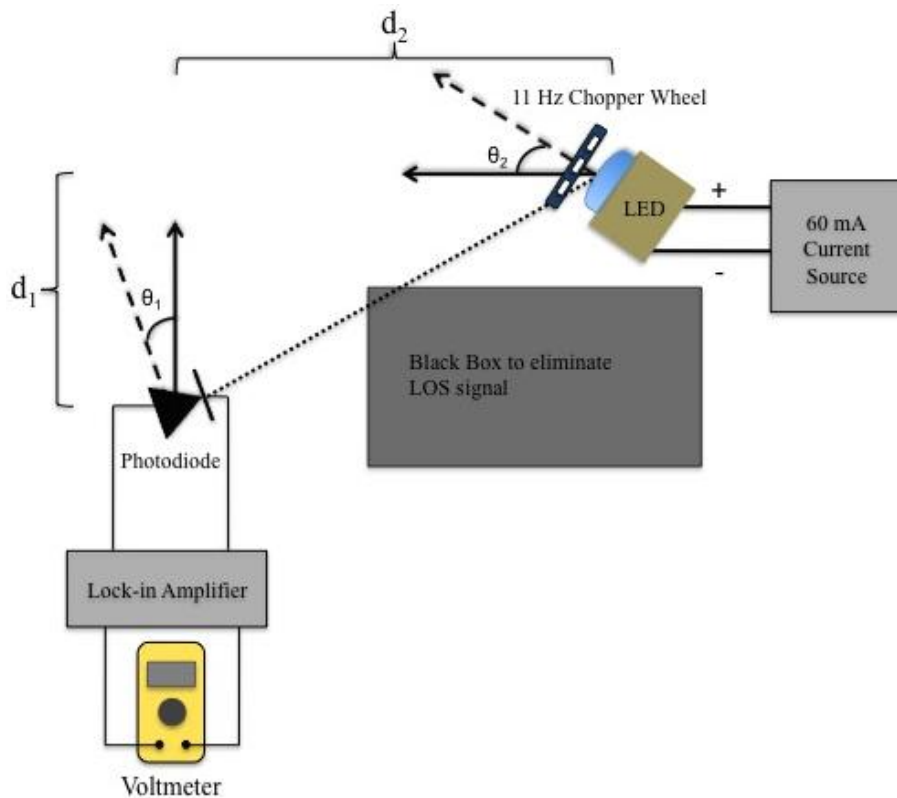


Figure 41. Setup used to measure intensity of UV light due to Rayleigh scattering.

Because the photodiode used for detection has no additional gain, an 11 Hz chopper was placed directly in front of the LED to modulate the emitted UV light and increase the sensitivity of detection. The signal from the photodiode was then sent to a lock-in amplifier synchronized with the chopper, isolating the UV source from background noise.

Because the goal was to detect only those photons reaching the detector through scattering reactions, measures were taken to reduce any signal from either reflection or the direct LOS path. Because the measurements were taken in a laboratory setting, it was impossible to entirely eliminate all sources of reflection (reflection off of walls, table, etc.). However, other potential sources of reflection were removed from the area. Control tests to vary potential sources of reflection indicate that intensity due to reflected photons was small. To eliminate the LOS signal, a block was placed in the direct path between the source and detector.

The intensity of the scattered light was measured as the detector angle (θ_1) was increased in 10° increments beginning at 0° . This was done for emission angles (θ_2) of 0° , 30° , 60° , and 90° . In addition to varying the detector angle and emission angle, the relative position of the source and receiver were also changed. The measurements were first taken for $d_1 = d_2 = 6$ in. For the second set of measurements, the detector was moved back such that $d_1 = 12$ in, while d_2 remained at 6 in. For the final measurements, the source was moved back, making $d_2 = 12$ in, while d_1 was returned to 6 in. The results, shown in Figures 42-44, indicate that indeed Rayleigh scattering is occurring and being detected.

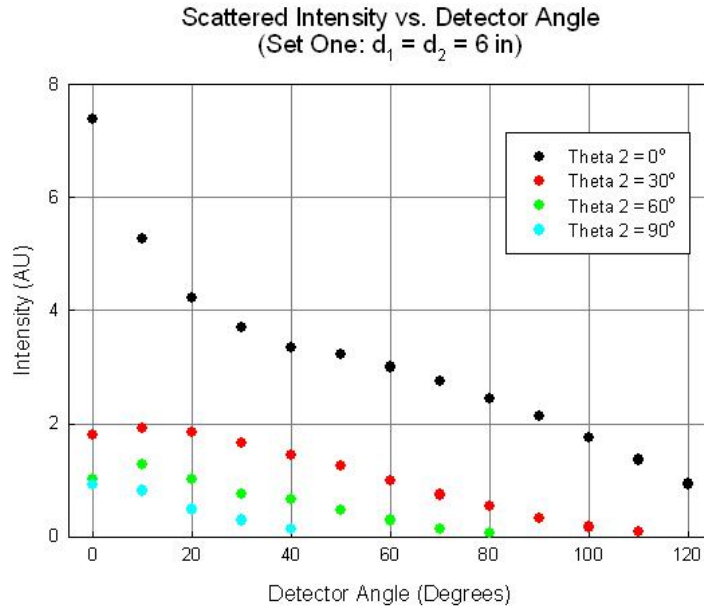


Figure 42. Scattered intensity as a function of detector angle for first measurement set ($d_1 = d_2 = 6$ in).

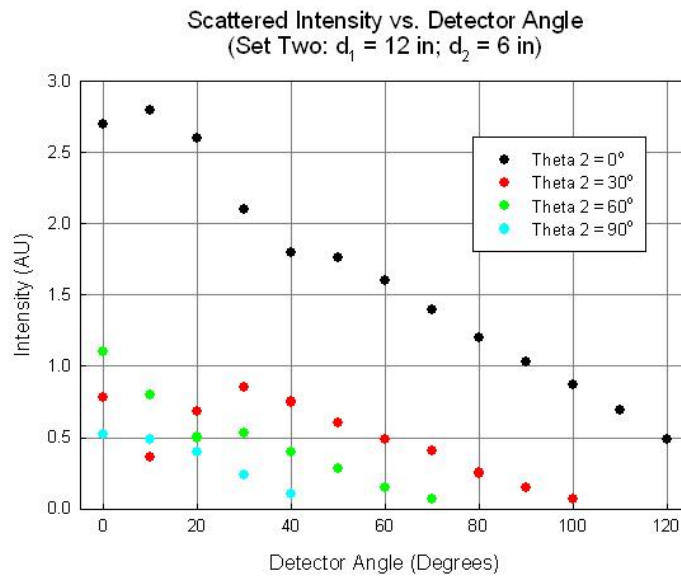


Figure 43. Scattered intensity as a function of detector angle for second measurement set ($d_1 = 12$ in; $d_2 = 6$ in). The irregularities for angles less than 20° are because a significant fraction of the detector's field of view does not contribute to intensity for small angles for this relative position between the source and receiver.

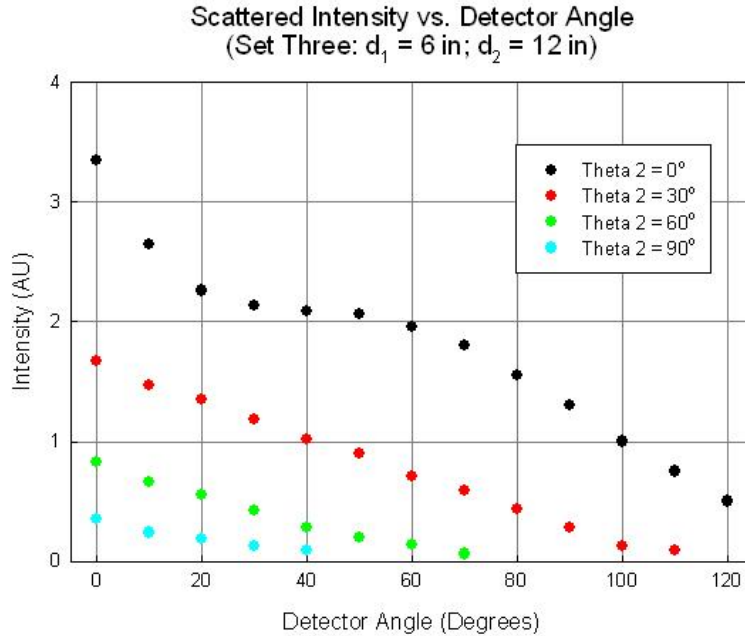


Figure 44. Scattered intensity as a function of detector angle for third measurement set ($d_1 = 6$ in; $d_2 = 12$ in).

The results suggest that the vast majority of the detected intensity is indeed due to Rayleigh scattering and not reflection. Had the signal been the result of reflection, the highest intensities would have been achieved when the source and detector were aimed in the same direction (i.e. $\theta_1 = 90^\circ$ and $\theta_2 = 0^\circ$; or $\theta_1 = 0^\circ$ and $\theta_2 = 90^\circ$). However, as expected, the measured intensity reached a higher values when the UV beam ran perpendicular to the detector's field of view. The only exception to this is for detector angles below 20° in set two. However, due to the relative positions of the source and receiver in set two, a significant portion of the detector's field of view does not contribute for small detector angles.

C. NLOS IMAGING

Using the intensified PentaMAX camera, attempts were made to produce images of UV beams scattering in air. To collect more light, these attempts incorporated the use of long exposure times. However, even in the absence of background light, exposure

times greater than five minutes caused the entire ccd array to become saturated. This is most likely due to thermal noise. Figure 45 shows an example of an attempt to view the beam of a 270 nm HS LED angled perpendicular to the camera's field of view.



Figure 45. Attempt to view scattering of UV photons in air.

Although Rayleigh scattering should occur, the intensified PentaMAX camera used to capture the image in Figure 45 is not sensitive enough to show this for regular room air conditions for the source intensity used in these experiments. To produce NLOS images of scattered solar blind UV light, a camera with higher gain and/or less noise must be used.

D. SUMMARY AND CONCLUSION

Although occurrences of Rayleigh scattering increase dramatically at shorter wavelengths ($\sim 1/\lambda^4$), this scattering did not produce the desired images when viewed with the intensified PentaMAX camera. However, in agreement with other research, scattered UV light was detected using a photodiode and lock-in techniques. Other research indicates that use of detectors with larger gain should enable detection of scattered photons from deep UV LEDs with intensity comparable to our prototype source at ranges in the 10's of meters.

THIS PAGE INTENTIONALLY LEFT BLANK

VI. SOLAR BLIND UV IIFF PROTOTYPE PERFORMANCE AND CONCLUSION

A. PROTOTYPE DESIGN

To develop a covert, solar blind UV IIFF patch, six models of deep-UV LEDs from SETI were analyzed. This research indicates that the 270 nm HS LED is the optimum UV source for the device. By driving the LEDs with a pulsed 70 mA current, the emitted power can be greatly increased without the risk of overheating. Using four LEDs driven with such a current, a handheld prototype was clearly visible via direct line of sight during both day and night at test distances of 300 m with indications of potentially much farther ranges. However, at this intensity, the capability of nonlinear of sight imaging is not feasible with the detection system used in this research.

The results of this baseline research were used to develop a functioning prototype IIFF device. The objective for this device was to be visible at 1 km during both day and night and to have the capability to operate in either trigger or beacon mode. Syvax Design designed the driving and detection circuitry for the prototype, which is shown in Figure 46.



Figure 46. Solar blind UV IIFF prototype device.

The emitter consists of four 270 nm HS LEDs, each driven with a 70 mA current. The current is pulsed with a frequency of 1.67 Hz and 50% duty factor. The device can function in one of two modes: beacon or trigger. If the patch is emitting in beacon mode, the signal is a continuous cycle of 300 ms on, 300 ms off pulses. While in trigger mode, the device is passive. Unless it detects that it is being targeted by a friendly, it remains completely covert; it will not respond if targeted by either enemy or neutral troops. If activated, the prototype responds by emitting ten 300 ms flashes followed by a return to passive mode.

The dimensions of the prototype are 6 ½” x 4 ½” x 1 ½”, with the majority of this space being occupied by the power supply. To accommodate the possibility of many hours of continuous use for testing, 9 AA batteries were used. Although this makes the prototype too large to function as a practical IIFF device, the primary purpose of the device is to test the range of visibility. Once the desired ranges have been achieved, necessary adjustments could be made to reduce the size of the device in order to construct a practical IIFF patch or signaling device.

B. PROTOTYPE PERFORMANCE AND EVALUATION

The prototype was tested at Camp Roberts, CA on the 1 km runway at McMillan airfield. The maximum test range was 980 m, where the device was clearly visible during both day and night. In addition, at this distance the prototype was successfully triggered by an IR laser in both twilight and full dark conditions. Using an IR laser for long range triggering requires the use of a NVD and therefore remote triggering was not achieved during the day. However, in future work on this project a properly modulated visible (red) laser could be easily developed and applied for daytime triggering.

Figure 47 shows both an individual and the device at 980 m as seen through both a visible camera as well as the UV capable intensified PentaMAX camera combined with the 270N and 270B solar blind filters.



Figure 47. Daytime images of prototype device viewed from 980 m by visible camera (Top) and intensified PentaMAX camera with 270N and 270B solar blind filters and 30 ms exposure time (bottom). In the second image, the prototype is the white dot shown just below the horizon.

Even with 4 x optical zoom used with the visible camera, neither the UV signal nor the individual are discernable at 980 m. However, even with no zoom the UV light

emitted by the prototype is clearly shown and provides a maximum pixel count of 510. Also, during live viewing the flashing of the signal causes it to be even more prominent.

Figure 48 shows a night image of the prototype taken by the intensified PentaMAX camera with the 270B solar blind filter and a 20 ms exposure from 980 m. The maximum pixel count in the image is 852.

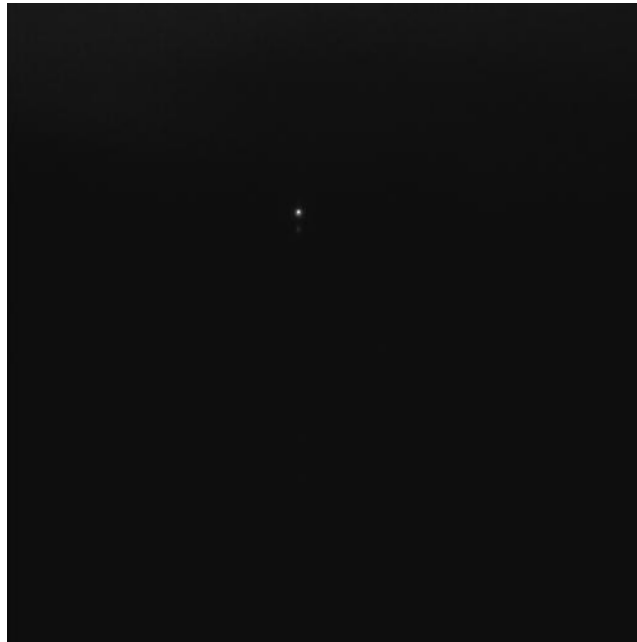


Figure 48. Nighttime image of prototype device viewed from 980 m with 20 ms exposure time.

C. CONCLUSIONS AND SUGGESTIONS FOR FUTURE WORK

The tests performed with the prototype demonstrate that an IIFF patch based in the solar blind UV region of the spectrum could function at long ranges both day and night. The first prototype was viewed successfully at a range of 1 km; future research on this project should be able to improve upon this performance.

One weakness of the prototype is that it is too large to be considered as a functioning IIFF device. However, future work on the project could reduce the size of the power supply, helping to develop a practical IIFF patch.

Another weakness of the prototype is that it depends heavily upon device orientation because LEDs with the HS lens were used in the design. Although the HS lens provides maximum intensity, the emission pattern of the light is very narrow. One possible solution to this problem for future designs might be to install each of the LEDs with a small offset angle. In addition, when the receiver is viewing the LEDs at an angle of more than 6° from the centerline, the BL lens provides the most intensity. Therefore, another possible solution is to incorporate the use of a combination of HS and BL model LEDs. Future research on this project will be able to determine the optimal design for attaining maximum direct line intensity while minimizing the dependence upon angle of orientation.

Another area for further research is that of utilizing photon scattering for NLOS imaging. Although the research presented here has shown that a NLOS signal does exist, the intensified PentaMAX camera used for the UV imaging was not able to create discernible NLOS images without the use of added large particulates in the air. However, this may be possible with a more sensitive camera and better optical filters. Additionally, a wide band gap camera that does not respond to background radiation in the visible part of the spectrum could eliminate the need for optical filters.

There is also a need for a working model to predict the NLOS intensity received through scattering reactions. This intensity depends upon the distance between the source and receiver, as well as the angles of each, and the overlap volume between the receiver field of view and emission beam. However, the exact dependence upon each of these factors needs to be systematically modeled.

Finally, although the unique properties of the solar blind region provide a zero solar background radiation condition, spatial context is not provided. This is evidenced in the multiple images captured in this research, particularly those captured at night. Another area for future work on this project could be to fuse the UV image with visible (day) or NIR (night) images to provide this spatial context. Efforts are currently being made by U.S. Special Operations Command (USSOCOM) to develop head mounted digital fusion goggles to provide situational awareness in all environments by utilizing

image fusion algorithms to combine a NIR sensor with a Long Wave IR (LWIR) sensor [17]. A natural evolution of this process would be to incorporate a solar blind UV sensor to provide enhanced situational awareness during both day and night operations.

APPENDIX. SUPPLEMENTAL



15 Discovery Way, Acton, MA 01720 USA
 Phone: (978) 263-3584 Fax: (978) 263-5086

QUOTATION

116682

Spencer Talley
 Naval Postgraduate School
 1 University Circle
 Monterey, CA 93943 US

Phone : +1 (831) 656-2023
Fax : +1 (831) 656-3238
Email : svtalley@nps.edu

Issue Date: August 10, 2010
Valid Until: September 10, 2010

Details:

Item	Part Number and Description	Customer Part Number	Rev.								
1	FN255-N-2D 255nm Narrowband Filter Peak Wavelength: 255nm +/- 2.5nm FWHM: 20nm +/- 5nm Minimum Peak Transmittance: 15%T Visible Rejection: Typically 10-4 Material: UV Grade Fused Silica DIA: 2.000" +0.000"/-0.005" THK: 4mm +0.25mm Surface Figure: 1-2 waves at 632.8nm, both surfaces Scratch Dig: 20-10 both surfaces Parallelism: 3 arc minutes Chamfer: 0.5mm x 45 deg. nominal Clear Aperture: Central 80%										
<table style="width: 100%; border-collapse: collapse;"> <thead> <tr> <th style="text-align: left;">Quantity</th> <th style="text-align: left;">Unit Price</th> <th style="text-align: left;">EA/LOT</th> <th style="text-align: left;">Lead Time</th> </tr> </thead> <tbody> <tr> <td style="text-align: left;">1.00</td> <td style="text-align: left;">\$560.00</td> <td style="text-align: left;">EA</td> <td style="text-align: left;">3 Weeks</td> </tr> </tbody> </table>				Quantity	Unit Price	EA/LOT	Lead Time	1.00	\$560.00	EA	3 Weeks
Quantity	Unit Price	EA/LOT	Lead Time								
1.00	\$560.00	EA	3 Weeks								

2 FB255-B-2D
 254nm Broadband Filter
 Peak Wavelength: 254+/-5nm
 FWHM: 40+/-10nm
 Min. Peak Transmittance: 30%T
 Visible Rejection: 10-2 to 10-4
 Material: UV Grade Fused Silica
 Dia.: 2.000" +0.000"/-0.005"
 Thk.: 4mm +0.25/-0.00mm
 Surface Figure: 1-2 waves @ 632.8nm, both surfaces
 Scratch Dig: 20-10 both surfaces
 Parallelism: 3 arc minutes or better
 Chamfer: 0.5mm x45 deg. nominal
 Clear Aperture: Central 80%

Quantity	Unit Price	EA/LOT	Lead Time
1.00	\$575.00	EA	3 Weeks

3 FN270-N-2D
 270nm Narrowband Filter
 Peak Wavelength: 270nm +/- 2.5nm
 FWHM: 20nm +/-5nm
 Minimum Peak Transmittance: 15%T
 Visible Rejection: Typically 10-4
 Material: UV Grade Fused Silica
 DIA: 2.000" +0.000"/-0.005"
 Thk: 4mm +/-0.25mm
 Surface Figure: 1-2 waves at 632.8nm, both surfaces
 Scratch Dig: 20-10 both surfaces
 Parallelism: 3 arc minutes
 Chamfer: 0.5mm x 45 deg. nominal
 Clear Aperture: Central 80%

Quantity	Unit Price	EA/LOT	Lead Time
1.00	\$560.00	EA	3 Weeks

4 FB270-B-2D

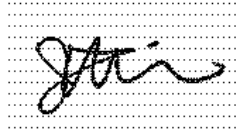
270nm Broadband Filter
Peak Wavelength: 270±5nm
FWHM: 45±10nm
Min. Peak Transmittance: 30% T
Visible Rejection: 10-2 to 10-4
Material: UV Grade Fused Silica
Dia.: 2.000" +0.000/-0.005"
Thk.: 4mm +0.25/-0.00mm
Surface Figure: 1-2 waves @632.8nm, both surfaces
Scratch Dig: 20-10 both surfaces
Parallelism: 3 arc minutes or better
Chamfer: 0.5mm ±45 deg. nominal
Clear Aperture: Central 80%

Quantity	Unit Price	EA/LOT	Lead Time
1.00	\$575.00	EA	3 Weeks

All prices in U.S. dollars, F. O. B.: Acton, MA
Sales tax will be added where appropriate
Payment Terms: Net 30 - subject to credit approval
Warranty: One year from date of shipment

Technical Inquiries: Joanne Choi +1 (978) 268-0337
Order Inquiries: Darren White +1 (978) 268-0306

Authorized by:



TERMS AND CONDITIONS OF SALE

Any quotation or sale by Princeton Instruments, a division of Roper Scientific, Inc., Acton Research Corporation, and their respective divisions and business units (herein referred to individually and collectively as "Seller") to any customer, distributor, original equipment manufacturer, end-user, or other purchaser (herein, "Purchaser") is made on the following terms and conditions. By accepting delivery of products sold hereunder ("Products"), Purchaser accepts and agrees to be bound by these Terms and Conditions, which will supersede any terms and conditions stated in any purchase order or similar document furnished by Purchaser. No modification of any of these terms and conditions shall be valid against any Seller unless the modifications appear in a document signed by an authorized officer of such Seller.

1. **Payment Terms; Interest.** Unless otherwise specified by Seller, payment terms are net 30 days from date of invoice by wire transfer to Seller's designated account, in United States dollars. Credit limits and extensions are subject to the review and approval of Seller, in its sole discretion. Seller reserves the right to change its terms of sale or to require prior payment, letter of credit or COD when, in the opinion of Seller, the financial condition or previous payment record of Purchaser so warrants. Seller shall not be obligated to extend credit to any Purchaser. Should Purchaser become delinquent in any payment due, Seller at its own discretion may institute credit hold procedures on all open orders. Future orders will not be confirmed until Purchaser's account is brought current, including outstanding interest charges, if any.

2. **Taxes & Duties.** Prices quoted by Seller are exclusive of all taxes, import/export duties, and surcharges applicable to the Products (including, without limitation, sales, use, value added, excise, property, customs and similar taxes or duties). Any such tax, fee, or charge shall be paid by the Purchaser in addition to the prices quoted or invoiced. All applicable taxes, duties, freight, and shipping charges will be separately stated on Seller's invoice in addition to the prices quoted or invoiced. Seller reserves the right to pass through surcharges, which shall be paid by Purchaser in addition to the prices quoted or invoiced.

3. **Acceptance and Cancellation of Orders.** Any quotations given by Seller will be valid for the period stated on the quotation. Orders for Products must be presented in writing or via electronic means acceptable to Seller and will not be binding upon Seller until accepted by written or electronic confirmation or by shipment of the Products ordered. Seller reserves the right, at its option and without liability, to refuse any order, in whole or in part, or to specify an alternate delivery schedule if orders from all sources exceed Seller's inventory or ability to deliver. Seller may allocate available inventory and production in its sole discretion. Accepted orders may be cancelled only if written notice is provided to Seller prior to shipment of any part thereof and only upon payment of such reasonable cancellation charges as Seller may request, which may include but not be limited to tooling and work-in-progress expenses.

4. **Product Shipment and Risk of Loss; Inspection.** All shipments are Ex-Works, per Incoterms 2000, unless otherwise specified in Seller's order acknowledgement. Seller will select the method of shipment and carrier. Risk of loss or damage passes to Purchaser upon issuance of the carrier's bill of lading, and Seller shall not be liable for any delays or loss or damage to Products in transit. Any claim for shortage, damage in transit or other nonconformance must be made directly to the delivering carrier within ten (10) days of receipt of shipment. If Purchaser fails to give timely notice, Products delivered shall be deemed to conform to Purchaser's order.

5. **Limited Warranty; Disclaimer.** Products sold by Seller are covered by Seller's standard, printed warranties provided with each product. Such warranties, including all limitations and exclusions therein, are incorporated herein by reference. Such warranties will be effective, and Seller will be obligated to honor such warranties, only upon Seller's receipt of payment in full for the product(s) to be warranted. Seller's warranties do not cover any product that Seller reasonably determines has been modified, misused, or abused, or any damage or defect due to relocation, accident, negligence, failure of electrical power, tampering, or failure to follow Seller's handling, operating and maintenance instructions. Products returned for repair or replacement under warranty shall be shipped with freight prepaid by Purchaser.

TO THE FULL EXTENT PERMITTED BY LAW, THE WARRANTY AND REMEDIES SET FORTH IN SELLER'S STANDARD PRINTED WARRANTIES ARE EXCLUSIVE AND IN LIEU OF ALL OTHER REPRESENTATIONS, WARRANTIES, TERMS, OR CONDITIONS, WRITTEN OR ORAL, EXPRESS OR IMPLIED, STATUTORY OR OTHERWISE, IN CONNECTION WITH THE DESIGN, SALE, INSTALLATION, OR USE OF SELLER'S PRODUCTS, INCLUDING WITHOUT LIMITATION ANY WARRANTIES, TERMS, OR CONDITIONS OF MERCHANTABILITY, FITNESS FOR A PARTICULAR PURPOSE, CORRESPONDENCE WITH DESCRIPTION, SATISFACTORY QUALITY, OR NONINFRINGEMENT, ALL OF WHICH ARE HEREBY EXPRESSLY DISCLAIMED. WHEN, UNDER APPLICABLE LAW, IMPLIED WARRANTIES MAY NOT BE EXCLUDED IN THEIR ENTIRETY, SUCH WARRANTIES WILL BE LIMITED TO THE DURATION OF THE APPLICABLE WRITTEN WARRANTY. COPIES OF THE SELLER'S STANDARD PRINTED WARRANTIES MAY BE OBTAINED UPON REQUEST.

IN NO EVENT SHALL SELLER BE LIABLE TO PURCHASER OR ANY THIRD PARTY FOR ANY OTHER DAMAGES ARISING OUT OF THE USE OF, OR INABILITY TO USE, SELLER'S PRODUCTS, OR FOR ANY OTHER DAMAGES WHATSOEVER, INCLUDING WITHOUT LIMITATION ANY SPECIAL, CONSEQUENTIAL, INCIDENTAL, INDIRECT, EXEMPLARY OR PUNITIVE DAMAGES OF ANY KIND, EVEN IF ADVISED OF THE POSSIBILITY THEREOF. SELLER'S TOTAL LIABILITY FOR DAMAGES, WHETHER IN CONTRACT, TORT, OR OTHERWISE, SHALL NOT EXCEED THE PURCHASE PRICE PAID BY PURCHASER FOR THE PRODUCTS COVERED BY THESE TERMS AND CONDITIONS.

REV 0509

6. **Purchase Money Security Interest.** Purchaser hereby grants to Seller a purchase money security interest in all Products purchased hereunder, and any proceeds received by Purchaser with respect thereto, as security for the payment of all amounts due from Purchaser to Seller. Upon request by Seller at any time, Purchaser agrees to assist Seller in executing and filing such financing statements or other documents as may be required to evidence and perfect such security interest in any jurisdiction.

7. **Return Policy.** Other than returns of Products pursuant to valid warranty claims, Products may be returned for refund or credit only with advance written approval and a Returned Materials Authorization ("RMA") number from Seller. An RMA Number may be obtained by contacting Seller's sales department. Proof of purchase is required. The RMA Number must appear on all shipping documents and related correspondence. Merchandise returned without such approval may be returned to Purchaser freight collect. Returned Products must have been purchased within twelve months prior to the date of return, and must be in the same condition as when they were shipped by Seller and in their original, unopened packaging. All returned merchandise must be sent by Purchaser freight prepaid and properly boxed to prevent damage in transit. **SELLER WILL NOT ACCEPT ANY C.O.D. PARCELS.** Seller will inspect the product upon receipt and issue the credit based on the age and condition of the merchandise and the terms of Seller's Returned Goods Policy. For any stock items returned, a restocking charge of up to twenty-five percent (25%) of the invoiced price may be charged. Special Order items (that are not stock items at Seller) are not returnable or refundable under any circumstances. After thirty (30) days, all sales are final.

8. **Force Majeure.** Seller shall not be liable or deemed to be in default for non-performance or delay in performance under these Terms and Conditions or any contract with Purchaser to the extent caused by any act of God or public enemy, war, riot, civil commotion, act of terrorism, fire, flood, epidemic, earthquake, accident, explosion, casualty, embargo, action of the elements, strike, lockout or labor dispute, governmental law, regulation, or ordinance, order of a court of competent jurisdiction, or any other cause beyond Seller's reasonable control.

9. **Other Documents & Terms.** Additional terms and conditions as found on Seller's quotations, acknowledgements and invoices are to be considered as part of these Terms and Conditions. If Purchaser has signed a separate purchase or supply agreement with Seller, the terms of that separate agreement shall govern over any conflicting terms herein. No purchase order or other document in any way modifying any of these Terms and Conditions will be binding upon Seller unless made in writing and signed by an authorized officer of Seller. Course of performance, course of dealing, and usage of trade shall not apply.

10. **Amendment.** These Terms and Conditions may be amended or modified by Seller at any time by delivering a copy of such modified Terms and Conditions to Purchaser. Any attempt to alter, supplement, or amend this document or enter an order for product(s) which is subject to additional or altered terms and conditions will be null and void, unless otherwise agreed to in a written agreement signed by both Purchaser and Seller.

11. **Finance Charges and Collection Expenses.** Any amounts due to Seller that are not paid on the due date therefore shall bear interest, from the date due until paid in full, at a rate equal to the lower of 1.5% per month or the highest legal rate, compounded monthly. If Seller deems it necessary or appropriate to refer an account to an agent or attorney for collection, all costs and expenses of collection (including, without limitation, reasonable attorneys' fees) will be charged to Purchaser's account and will accrue interest at the rate stated above. Seller may set off against any sum otherwise due from Seller to Purchaser or its affiliates any sums or amounts then due from Purchaser and its affiliates to Seller and its affiliates.

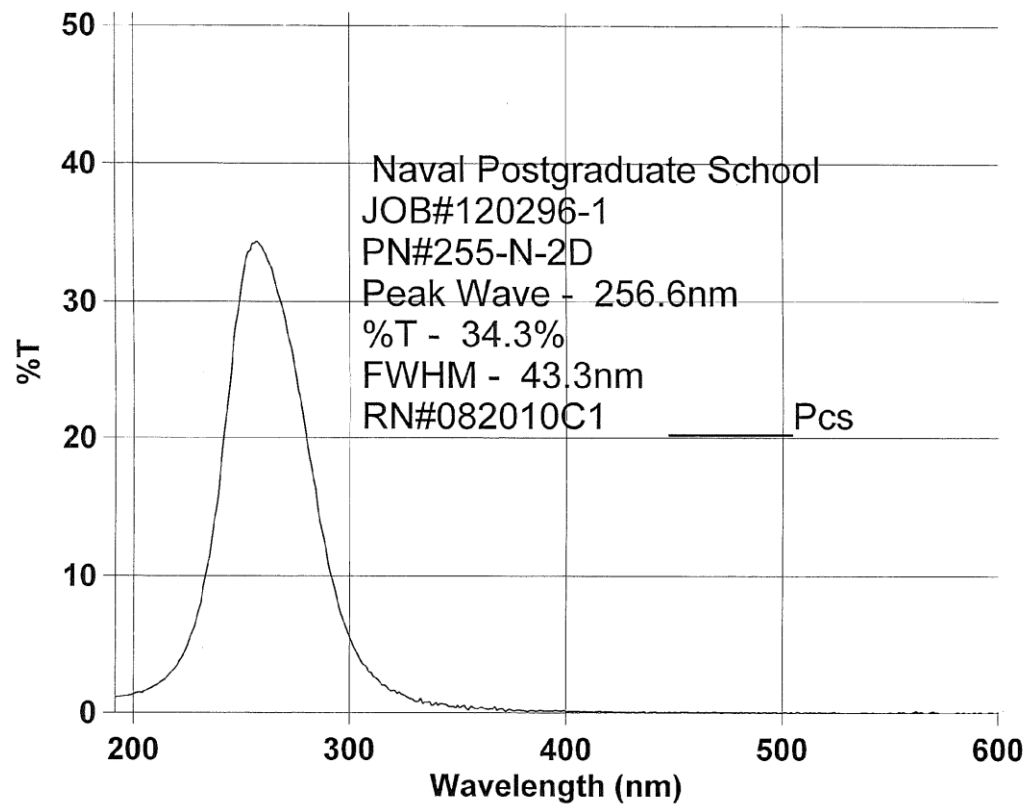
12. **Compliance with Laws.** Purchaser is responsible for compliance with any laws, regulations and legal authorities applicable to the purchase, export, import, transfer, sale or other disposition of the purchased Products, including all applicable U.S. export control laws and regulations, and shall not export, re-export, or otherwise transmit, directly or indirectly, any Product, software, technical data, or other materials received from Seller, or the direct products thereof, unless in full compliance with all applicable laws and regulations, including obtaining any required export licenses. If Purchaser requires Seller to export Products from the U.S., Purchaser will be responsible for providing all import certificates or other documents necessary to obtain any required export licenses.

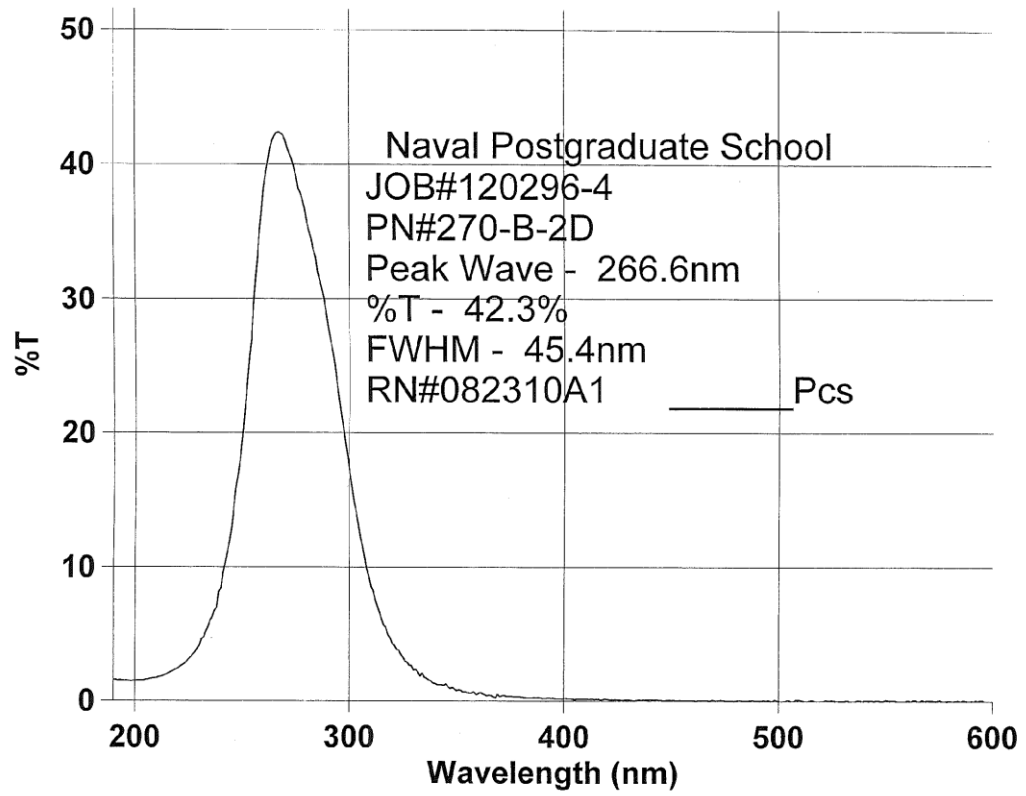
13. **Governing Law & Jurisdiction.** These Terms and Conditions and all transactions hereunder (including without limitation any disputes arising out of deliveries from Seller to Purchaser) shall in all respects be governed by and interpreted and enforced in accordance with the laws of the State of Delaware and the United States of America, without giving effect to any conflict of law provision that would cause the application of the laws of any other jurisdiction. To the extent the United Nations Convention on Contracts for The International Sale of Goods could be applicable by operation of the laws of Delaware, Seller and Purchaser hereby opt out of the application of the Convention and any applicable international discovery and service of process conventions shall not be applicable. Purchaser consents to the jurisdiction of any court located in the State of New Jersey or in the Commonwealth of Massachusetts with respect to any legal action or proceeding to enforce any provision of, or based on any right arising out of, these Terms and Conditions and waives any objection to venue laid therein.

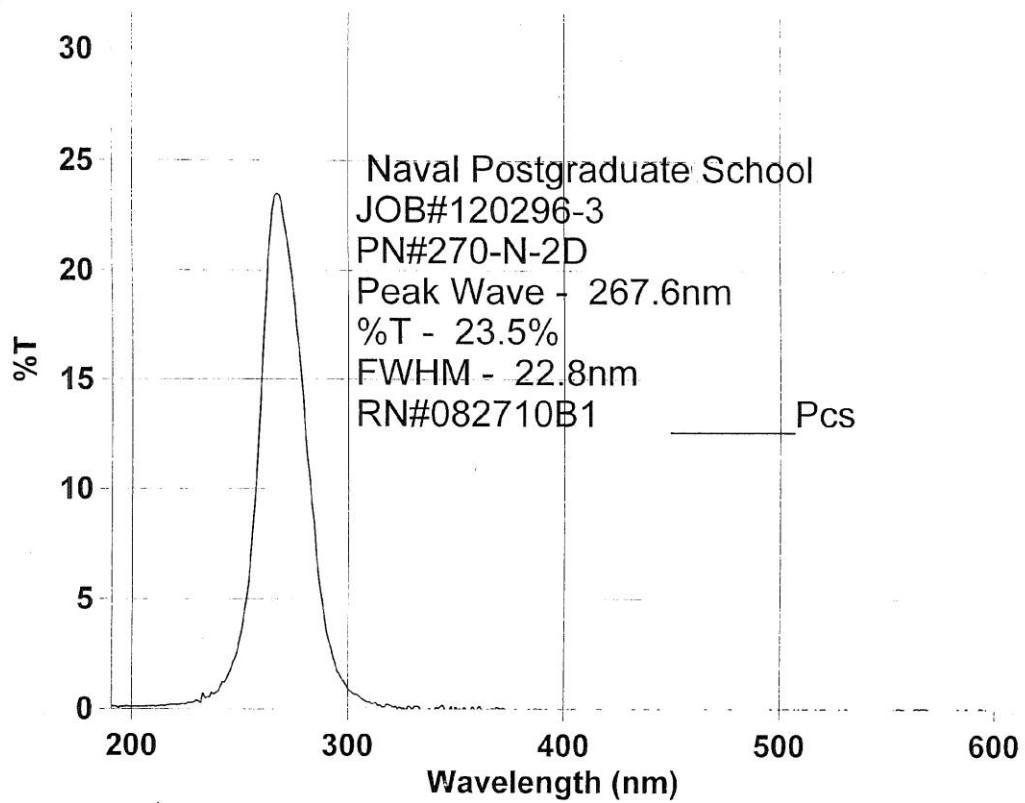
14. **Miscellaneous.** The rights and remedies of Seller herein are cumulative and in addition to all other rights and remedies available at law or in equity. Any failure to enforce any provision of these Terms and Conditions may not be construed as a waiver of such provision or any other provision nor of the right to enforce such provision. The invalidity, in whole or in part, of any provision hereof shall not affect the remainder of the provisions. Any waiver or renunciation of a claim or right arising out of breach must be in writing and signed by the injured party.

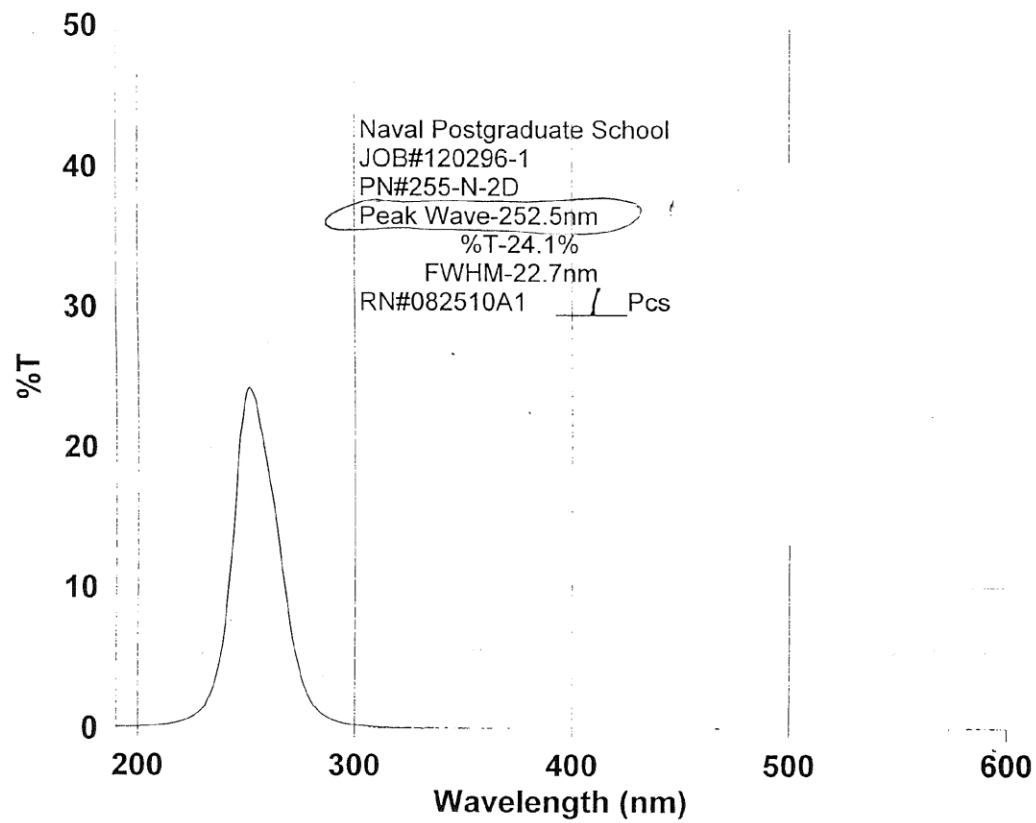
15. **Headings.** The section headings used herein are for convenience of reference only, and may not be used in the interpretation hereof.

REV 0509









THIS PAGE INTENTIONALLY LEFT BLANK

LIST OF REFERENCES

- [1] Defense Update, “Eliminating Fratricide in Ground Combat,” <http://defense-update.com/features/du-2-04/feature-fratricide.htm> (last accessed 20 May 2011).
- [2] K. Burger, “US Army shares radios to avoid Gulf fratricide,” *Jane’s Defense Weekly*, 12 March 2003.
- [3] R. Pengelley, “Cutting through the fog of war: armed forces strive to reduce fratricide threat,” *International Defense Review*, 01 May 2006.
- [4] “FY09 Technology Transition Initiative Projects” from Office of Secretary of Defense Web http://www.acq.osd.mil/ott/tti/FY09_projects.htm (last accessed 20 May 2011).
- [5] S. R. Gardner, “Visible-to-SWIR Downconversion and its Application to Individual Identification Friend or Foe (IIFB),” Naval Postgraduate School, June 2009.
- [6] A. L. Woolsey, “Short Wave Infrared (SWIR) Emission Using Erbium Doped Phosphors,” Naval Postgraduate School, June 2010.
- [7] R. D. Hudson, “Critical Review of Ultraviolet Photoabsorption Cross Sections for Molecules of Astrophysical and Aeronomical Interest,” *Reviews of Geophysics and Space Physics*, May 1971.
- [8] Ocean Optics Corporation, www.oceanoptics.com/Products/usb4000uvvis.asp, USB4000-UV-VIS datasheet, (last accessed 20 May 2011).
- [9] Acton Optics & Coatings, Quotation #116682, 10 August 2010 (Provided in Supplemental).
- [10] Z. Xu and B. M. Sadler, “Ultraviolet Communications: Potential and State-of-the-Art,” *IEEE Communications Magazine*, May 2008.
- [11] D. M. Reilly, D. T. Moriarty and J. A. Maynard, “Unique properties of solar blind ultraviolet communication systems for unattended ground sensor networks,” *Proceedings of SPIE Vol. 5611*.
- [12] R. Gaska and J. Zhang, “Deep-UV LEDs: Physics, Performance and Applications,” *Proc. SPIE* **6037** 603706.
- [13] G. Chen, Z. Xu, H. Ding, and B. M. Sadler, “Path loss modeling and performance trade-off study for short-range non-line-of-sight ultraviolet communications,” *Optics Express*, 02 March 2009.

- [14] Thorlabs Corporation, "Product Specification Sheet," FGAP71 Datasheet, 16 June 2010.
- [15] Sensors Electronic Technology Corporation, "UVTOP[®] Technical Data," UVTOP270 Datasheet, 2008.
- [16] M. Snee and W. Ubachs, "Direct Measurement of the Rayleigh Scattering Cross Section in Various Gasses," Journal of Quantitative Spectroscopy & Radiative Transfer, 2005.
- [17] Solicitation number H92222-10-DFG from Office U.S. Special Operations Command Web
https://www.fbo.gov/index?s=opportunity&mode=form&id=d06da10b8b21d09ac11987d15b3e2733&tab=core&_cview=1 (Last Accessed 20 May 2011).

INITIAL DISTRIBUTION LIST

1. Defense Technical Information Center
Ft. Belvoir, Virginia
2. Dudley Knox Library
Naval Postgraduate School
Monterey, California
3. Professor Andres Larraza
Naval Postgraduate School
Monterey, California
4. Professor Nancy M. Haegel
Naval Postgraduate School
Monterey, California
5. Professor Richard M. Harkins
Naval Postgraduate School
Monterey, California
6. LT Spencer Talley
Naval Postgraduate School
Monterey, California